

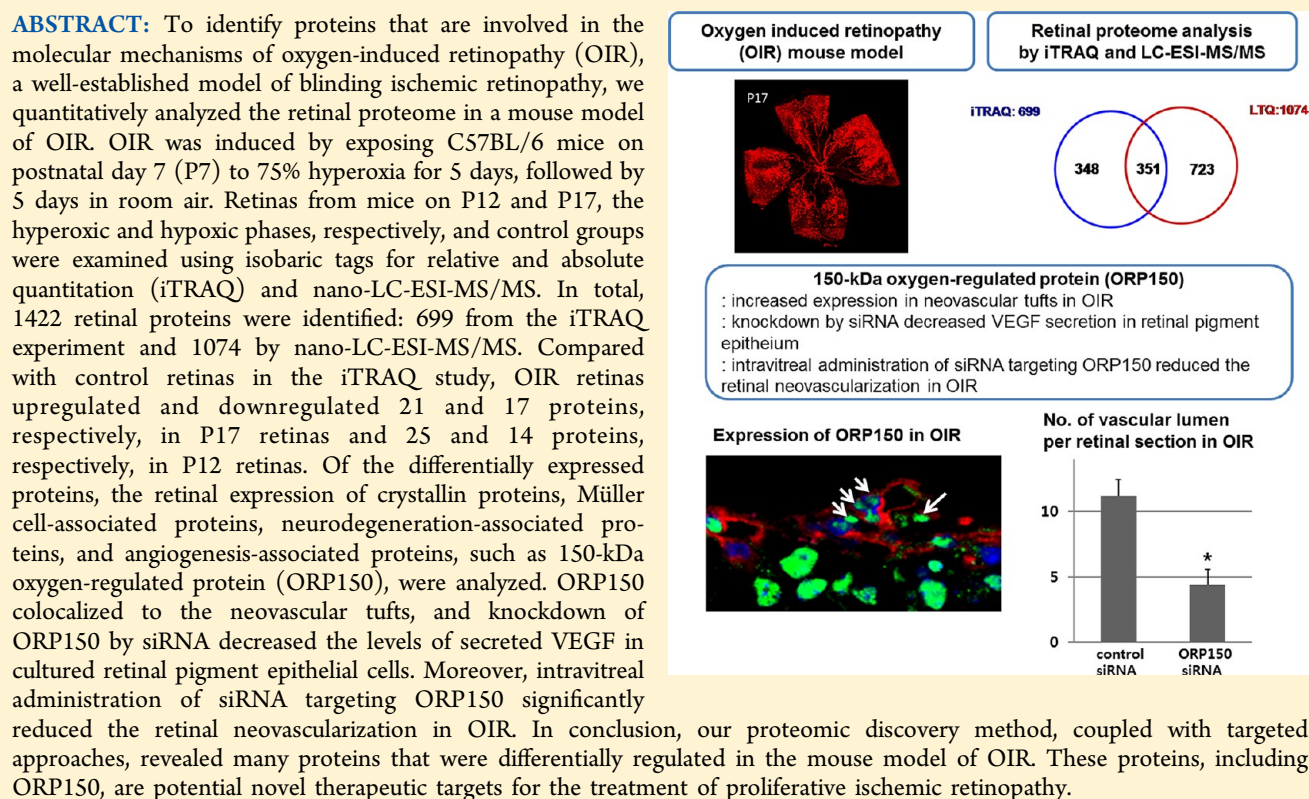
Retinal Proteome Analysis in a Mouse Model of Oxygen-Induced Retinopathy

Sang Jin Kim,^{†,§,#} Jonghwa Jin,^{‡,§,#} Young Joo Kim,[†] Youngsoo Kim,^{*,‡} and Hyeong Gon Yu^{*,†}

[†]Departments of Ophthalmology and [‡]Biomedical Engineering, Seoul National University College of Medicine, Seoul, Republic of Korea

[§]Department of Ophthalmology, Samsung Medical Center, Sungkyunkwan University School of Medicine, Seoul, Republic of Korea

Supporting Information



INTRODUCTION

Ischemic retinopathies, such as retinopathy of prematurity, proliferative diabetic retinopathy, and retinal vein occlusion, are major causes of permanent blindness.^{1–3} They present as abnormal retinal vascular proliferation, which leads to blinding complications, such as hemorrhage and retinal detachment.

Several proangiogenic factors, including vascular endothelial growth factor (VEGF), insulin-like growth factor, and erythropoietin, and antiangiogenic factors, such as Angiostatin and pigment epithelium-derived factor, have been identified, the imbalance of which mediates the pathogenesis of retinopathy.^{1,4–8} In addition, proteins that are related to inflammation, oxidative stress, and neuronal dysfunction might contribute to the molecular pathogenesis of ischemic retinopathy.^{9–12} However, the pathogenic mechanisms of

ischemic retinopathy are not fully understood, rendering the treatment challenging.

Proteomic platforms are useful for making unbiased discoveries of pathogenic factors that mediate ischemic retinopathy. Using isobaric tags for relative and absolute quantitation (iTRAQ), in which reporter ions are differentially and isotopically labeled, the relative concentrations of specific peptides can be determined from mixtures of complex proteins.

The iTRAQ technique has several advantages, such as its multiplexing capability, enabling simultaneous quantitation; relatively small intraexperimental variability; and higher sensitivity compared with other commonly used quantitation

Received: April 25, 2012

Published: October 5, 2012



techniques, such as isotope-coded affinity tags and 2-dimensional difference in-gel electrophoresis.¹³ Through proteomic methods that incorporated 2-dimensional gel-based proteomic analysis, iTRAQ, and nano-LC-ESI-MS/MS, several factors that might be related to the pathogenesis of diabetic retinopathy were identified in vitreous and plasma samples from diabetic patients and retinal tissues from diabetic animal models.^{14–20}

Oxygen-induced retinopathy (OIR) is a well-established animal model of blinding ischemic retinopathy.^{1,21–24} In the mouse model of OIR, neonatal mice are exposed to 75% hyperoxia from the postnatal day 7 (P7) until P12. During this phase, hyperoxic environment inhibits the retinal vessel growth and causes the degeneration of the existing blood vessels, which are apparent at P12. On returning to room air, the vascular retina becomes relatively hypoxic and triggers the production of angiogenic factors, which effects pathological angiogenesis. During the hypoxic phase, neovascularization develops and reaches its maximum at P17. Because the OIR model shares end results with human ischemic retinopathies, i.e., capillary loss and subsequent hypoxia-induced retinal neovascularization, it has been used widely to examine the pathogenic mechanisms of ischemic retinopathies and evaluate new therapeutic agents.^{1,21–24} Thus, a proteomic study that uses the OIR model might identify candidate proteins that are involved in the mechanisms of ischemic retinopathy, thereby constituting novel therapeutic targets. However, the retinal proteome in OIR has not been studied comprehensively.

In this study, to identify proteins that are related to the molecular mechanisms of OIR, we profiled the retinal proteome of the OIR mouse model by nano-LC-ESI-MS/MS and quantified retinal proteins by iTRAQ labeling, coupled with LC-MS/MS. Of the proteins that were differentially expressed between control and OIR retinas, we selected proteins that were suspected of being associated with angiogenesis, retinal vascular changes, and neurodegeneration in OIR, and performed a detailed characterization using targeted methods.

One such protein, ORP150, was upregulated in OIR and colocalized to neovascular tufts. The knockdown of ORP150 by siRNA downregulated secreted VEGF levels in cultured retinal pigment epithelial cells, implicating ORP150 in pathological retinal angiogenesis. Moreover, intravitreal administration of siRNA targeting ORP150 significantly reduced the retinal neovascularization. Overall, the proteomic discovery method, coupled with targeted approaches, revealed many differentially regulated proteins in the mouse model of OIR. These proteins, including ORP150, might be novel therapeutic targets for the treatment of proliferative ischemic retinopathy.

MATERIALS AND METHODS

OIR Mouse Model

OIR was induced as described.^{21,23} Briefly, newborn C57BL/6 mice were randomly assigned to experimental and control groups. On postnatal day 7 (P7), the pups and their nursing mothers were placed in a 75% oxygen atmosphere. The oxygen concentration was maintained with a Pro-Ox 110 oxygen controller (Bio-Spherix, Redfield, NY, USA). To serve as a CO₂ quencher, 50 g of soda lime was placed at the bottom of the chamber. The pups were returned to room air on P12. The mice were sacrificed on P12 and P17, and the eyes were enucleated. The control groups were subjected to room air until sacrifice. Mice that weighed less than 6 g on P17 were excluded

from the analysis due to possible alterations in vascular phenotype.²³

Mice were divided into 4 groups: control groups that were enucleated on P12 (P12C) and P17 (P17C) and OIR groups that were enucleated on P12 (P12) and P17 (P17). To confirm the development of OIR, retinal flat mounts ($n = 8$ eyes per groups) and paraffin-embedded retinal sections ($n = 10$ eyes per groups) were generated. After staining the retinal vessels with TRITC-labeled BS-1 lectin (LS264, Sigma Aldrich, St. Louis, MO, USA), we evaluated the retinal vaso-obliteration in P12 retinas and vascular regrowth and neovascularization in P17 retinas by confocal microscopy (LSM 500, Carl Zeiss MicroImaging GmbH, Germany). All animal experiments were conducted per the ARVO Statement for the Use of Animals in Ophthalmic and Vision Research and approved by the IACUC of Biomedical Research Institute, Seoul National University Hospital.

Retinal Protein Extraction

After enucleation, the retinas were isolated carefully under a dissecting microscope. After the cornea was secured, the sclera was peeled away toward the optic nerve with dissecting forceps. The sclera, optic nerve, and retinal pigment epithelium were then removed. Finally, we removed the retina from the lens and vitreous, carefully ensuring the lens integrity.

Proteins were extracted from the 4 groups of retinas ($n = 22$ eyes per group). The retinas in each group were pooled and homogenized in ice-cold PBS with protease inhibitor cocktail (Roche Complete Mini Tablets, Roche Applied Sciences, Indianapolis, IN, USA) by sonication and freeze-thaw lysis method. Protein concentrations were measured with Pierce BCA reagent (Thermo Scientific, Rockford, IL, USA). The 4 groups of pooled protein samples were used for iTRAQ experiment, LC-ESI-MS/MS analysis, and Western blot analysis.

iTRAQ Experiment

The iTRAQ technique was used to compare protein expression profiles in OIR tissues between P12 and P12C, between P17 and P17C, and between P17 and P12, allowing us to perform a comprehensive analysis of differential proteome expression by comparing the 4iTRAQ reporter ions. iTRAQ labeling and fractionation were performed as described.^{25,26}

One hundred micrograms of protein was labeled with iTRAQ reagents, and the proteins were reduced, alkylated, digested, and labeled per the manufacturer's instructions (Applied Biosystems, Foster City, CA, USA). For iTRAQ labeling, the 4 groups of retinas, P12C, P17C, P12, and P17, were labeled with iTRAQ reagents 114, 115, 116, and 117, and the 4 sample sets were combined and dried. The iTRAQ experiments were performed in triplicate with the same samples. The labeled iTRAQ samples were separated into 45 fractions by strong cation exchange (SCX) chromatography on an Agilent 1100 (Agilent Technologies, Palo Alto, CA, USA) with an SCX column (4.6 mm ID × 100 mm, 5 μm, 200 Å, PolyLC, Columbia, MA, USA).

The labeling efficiency was determined as described.^{25,26} Briefly, all possible labeling sites (the N-termini of all peptides and lysine side chains) in the 2437 peptides were compared manually with completely labeled sites, as represented using the Pro Group Algorithm in ProteinPilot (Applied Biosystems; MDS-Sciex, Concord, Canada).²⁷

LC-MS/MS experiments were performed as described.^{25,26} LC-MS/MS was performed using an integrated system, which

comprised an autosampler switching pump and a micropump (Tempo Nano LC system; Applied Biosystems) with a hybrid quadrupole-TOF LC-MS/MS spectrometer (QStar Elite; Applied Biosystems) that was equipped with a nanoelectrospray ionization source (Applied Biosystems). For each LC-MS/MS run, 1 μ g of fractionated peptides was injected into the LC-MS/MS system, where the peptides were trapped and concentrated on an Agilent Zorbax 300SB-C18 column (300 μ m ID \times 50 mm, 5 μ m, 100 \AA , Agilent Technologies). The peptide mixture was separated on an Agilent Zorbax 300SB nanoflow C18 column (75 μ m ID \times 150 mm, 3.5 μ m, 100 \AA , Agilent Technologies) at a flow rate of 300 nL/min. Solvent A and B consisted of ACN/water (2/98% (v/v)) with 0.1% formic acid and ACN/water (98/2% (v/v)) with 0.1% formic acid, respectively. The solvent gradient was started at 98% solvent A and 2% solvent B, and solvent B was gradually increased from 2 to 35% for 120 min, 35 to 90% for 10 min, and finally 90% for 15 min.

Eluted peptides were electrosprayed through a coated silica tip at 2300 eV (ion spray voltage). For the information-dependent acquisition (IDA), a survey scan was performed for the precursor ions for a 1-s period in the 400–1600 m/z mass range, and the five most abundant peptides (+2 to +4 charge states) that exceeded 20 counts were selected for MS/MS (100–2000 m/z mass range). Each selected fragment target ion was dynamically excluded for 60 s. The mass tolerance was set at 100 ppm.

MS Data Analysis and Gene Ontology Analysis

The data analysis was performed as described.^{25,26} Data file processing, protein identification, and relative abundance quantitation were performed using ProteinPilot v.2.0.1 and the Paragon algorithm. Database searches were performed against the mouse database (mouse combined_KBMSS.0.20050302.fasta was provided by Applied Biosystems). The following search parameters for identification and quantitation were used: a peptide and fragment ion mass tolerance of 0.2 Da, 1 missed trypsin cleavage, variable oxidation of methionine, fixed cysteine modification by MMTS, and iTRAQ labeling of the N-termini of peptides and lysine side chain residues. In this study, an unused ProtScore > 1.3 (95% confidence interval) was the confidence threshold for protein identification.

The “biological process” and “molecular function” classifications were analyzed using PANTHER ID numbers (<http://www.pantherdb.org/>). To analyze entire protein profiles more effectively, we performed a hierarchical clustering (HLC) and subclustering analysis on differentially expressed proteomes using MultiExperiment Viewer (<http://www.tm4.org/mev/>).²⁸

LC-ESI-MS/MS Analysis

Retinal proteins were analyzed by LC-MS/MS on an EasyLC (Proxeon, Odense, Denmark), which was coupled to a high-throughput tandem mass spectrometer (LTQ Velos, Thermo, Waltham, MA, USA) that was equipped with a nanoelectrospray device and fitted with a 10- μ m fused silica emitter tip (New Objective, Woburn, MA, USA). To generate the nanoflow LC gradient, solvent A (0.1% formic acid and 2% acetonitrile in double-distilled H₂O) and solvent B (98% acetonitrile with 0.1% formic acid) were used (0–40% solvent B over 76 min, followed by a gradient of 40–90% for 12 min and 90–100% over 5 min) at a flow rate of 300 nL/min.

The spray voltage was 1.8 kV in the positive ion mode, and the temperature of the heated capillary was 200 °C. For MS2,

Top 10 was implemented. A cycle of 1 full-scan MS survey spectra (m/z 300–1800) was acquired in the profile mode. Fragmentation of the precursor and detection of the product ions occurred in the linear trap in a data-dependent manner for the 10 highest-intensity ions. Only MS precursors that exceeded a threshold of 1000 ion counts were allowed to trigger MS/MS fragmentation.

All MS/MS spectra were acquired using the following parameters: normalized collision energy, 35; ion selection threshold, 1000 counts; activation Q, 0.25; and activation time, 10 ms. Dynamic exclusion was used with a repeat count of 1, a 15-s repeat duration, an exclusion list size of 50, an exclusion duration of 30 s, and ± 1.5 m/z exclusion mass width. Instruments were controlled through Tune 2.6.0 and Xcalibur 2.1 (Thermo Finnigan, San Jose, CA, USA).

Criteria for Protein Identification

All MS/MS spectra from LTQ Velos were analyzed using SEQUEST (Thermo Fisher Scientific, San Jose, CA, USA; version v.27, rev. 11), using the mouse database Uniprot-mouse.FASTA (147 548 entries). SEQUEST parameters for identification and quantitation were set by a fragment ion mass tolerance of 1.00 Da, a parent ion tolerance of 1.5 Da, carbamidomethylation of cysteine (fixed modification), and oxidation of methionine (variable modification).

Scaffold version Scaffold_3_00_03 (Proteome Software, Inc., Portland, OR, USA) was used to validate all MS/MS-based peptide and protein identifications. We selected peptides with greater than 95.0% probability, as specified by the Peptide Prophet algorithm.²⁹ Moreover, we used specific database search engine thresholds to validate the MS/MS-based peptides. SEQUEST identifications required at least deltaCn scores of greater than 0.10 and XCorr scores of greater than 1.8, 2.8, and 3.8 for singly, doubly, and triply charged peptides, respectively. All identified proteins were satisfied by greater than 95.0% probability and at least 2 identified peptides.³⁰

Immunofluorescence Staining

Eyes ($n = 10$ eyes per group) were enucleated, immersed in 4% paraformaldehyde for 24 h, and embedded in paraffin. Four-micrometer-thick serial sections were prepared from paraffin blocks. After deparaffinization and hydration, sections were incubated for 1 h in a blocking solution that was obtained from the same species in which the secondary antibody was developed. The slides were incubated with primary antibodies, as detailed in Table S1, Supporting Information.

After being washed with PBS, the slides were incubated for 1 h with Alexa Fluor 488 goat antimouse IgG (1:400, Invitrogen Molecular probes, Eugene, OR, USA), Alexa Fluor 488 goat antirabbit IgG (1:400, Invitrogen Molecular probes), or Alexa Fluor 555 donkey antigoat IgG (1:700, Invitrogen Molecular probes). Blood vessels were stained with TRITC-labeled BS-1 lectin (L5264, Sigma Aldrich), and cell nuclei were counterstained with DAPI. The stained sections were examined by confocal microscopy.

Western Blot

Each protein sample (10–30 μ g) was separated on a 4–12% Bis-Tris gel (NuPAGE Novex, Invitrogen) and transferred onto a PVDF membrane (Millipore, Billerica, MA, USA). The membranes were blocked with 5% skim milk in TBS-T (20 mM Tris-base, 150 mM NaCl, pH 7.4) and incubated with primary antibodies, rabbit anticrystallin α B (1:500), rabbit anticrystallin α B P-Ser-59 (1:500), rabbit anti-ORP150 (1:1000), rabbit

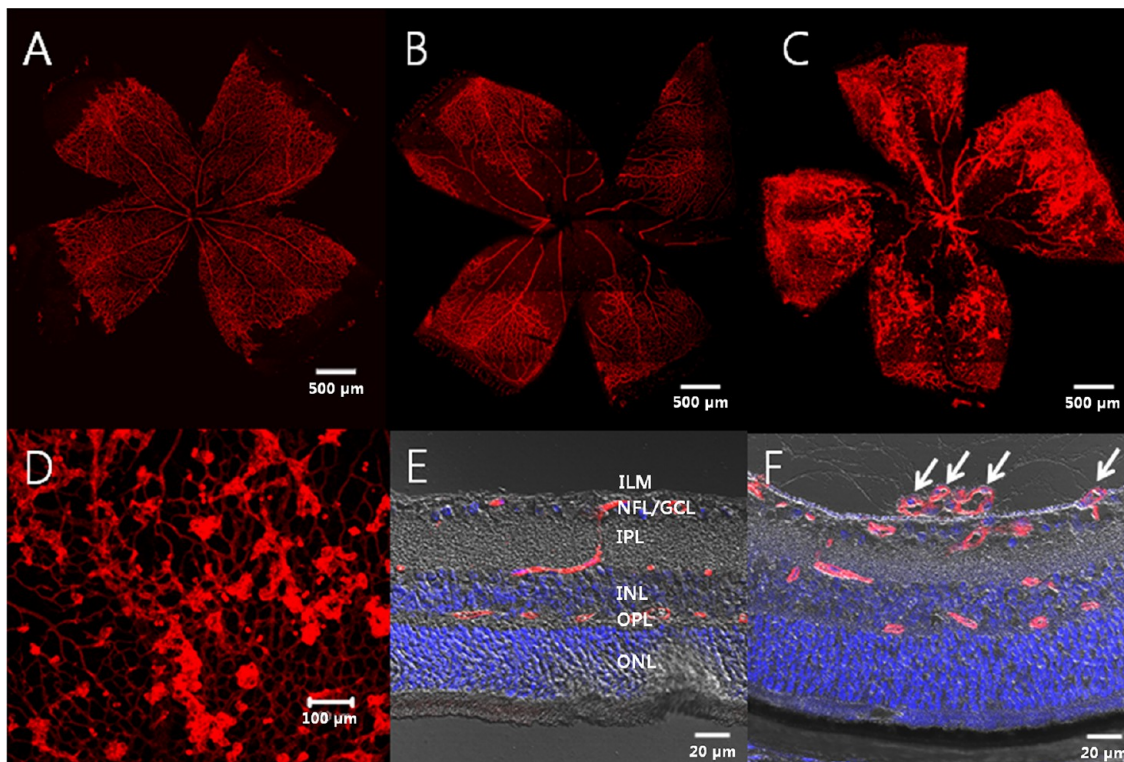


Figure 1. Confocal micrographs of flat-mounted and sectioned retinas from the mouse model of oxygen-induced retinopathy. On postnatal day 7 (P7) (A), when retinal vessels were not fully developed, mice were exposed to 75% oxygen, which effected significant vascular loss, shown in (B), by P12. After returning to room air on P12, the avascular retina became hypoxic, triggering neovascularization, peaking on P17 (C and D). Note the neovascular tufts (red, arrows) on the vitreal side of the internal limiting membrane on P17 (F) in contrast to the normal retinal vasculature in the P17 control (red, E). In (E) and (F), the nuclei were counterstained with DAPI (blue). ILM, internal limiting membrane; NFL/GCL, nerve fiber layer/ganglion cell layer; IPL, inner plexiform layer; INL, inner nuclear layer; OPL, outer plexiform layer; ONL, outer nuclear layer. Scale bars: (A–C), 500 μ m; (D), 100 μ m; (E) and (F), 20 μ m.

anticarbonic anhydrase II (CA II, 1:25,000), and rabbit anticarbonic anhydrase XIV (1:100). After a wash step, antirabbit IgG-alkaline phosphatase secondary antibody (1:20,000, Sigma Aldrich), was added for 1 h at room temperature. The antibody reactions were visualized using Fast BCIP/NBT alkaline phosphatase substrate (Sigma Aldrich). Western blots for Crystallin α B, Crystallin α BP-Ser-59, CA II, and ORP150 were performed in triplicate. The Western blots were scanned, and relative band densities were calculated using ImageJ (National Institutes of Health, Bethesda, MD, USA). The values between the groups were compared with the Mann–Whitney U test using SPSS for Windows (version 18.0, SPSS Inc., Chicago, IL, USA).

ELISA of VEGF from ORP150 siRNA-Treated ARPE-19 Cell Line

ARPE-19 cells (American Type Culture Collection, Rockville, MD, USA), a spontaneously immortalized human retinal pigment epithelial cell line, were maintained in DMEM-F12 medium, containing 10% fetal bovine serum (FBS). We seeded a 6-well culture plate with 2×10^5 cells per well in 2 mL of antibiotic-free DMEM-F12 medium that was supplemented with FBS.

ARPE-19 cells were transfected with control siRNA (sc-37007, Santa Cruz Biotechnology, Santa Cruz, CA, USA) or ORP150 siRNA (sc-96695, Santa Cruz Biotechnology), a pool of 3 target-specific 19–25-nt siRNAs that were designed to knock down gene expression, per the manufacturer's protocol. Briefly, ARPE-19 cells were incubated at 37 °C in a CO₂

incubator until the cells were 60–80% confluent. The siRNA transfection reagent mixture was added to the cells to 500 nM or 1 μ M. After a 6-h incubation, the medium was replaced with fresh DMEM-F12 medium.

After an additional incubation for 24 h, the supernatants of the cultures were harvested to measure secreted VEGF levels using a human VEGF ELISA kit (Thermo Scientific) per the manufacturer's protocol. To validate the knockdown of ORP150, proteins that were extracted from the cell lysates were analyzed by Western blot for ORP150 using rabbit anti-ORP150 (1:1000, Epitomics, Burlingame, CA, USA). The Western blots were scanned, and relative band densities were calculated using ImageJ.

Intravitreal Administration of siRNA against ORP150 in OIR

To assess the antiangiogenic effect of ORP150 inhibition, we intravitreally injected ORP150 siRNA (550 ng/1 μ L, sc-96695, Santa Cruz Biotechnology) diluted in lipid-based in vivo transfection reagent (Altogen Biosystems, Las Vegas, NV, USA) in one eye and control siRNA (sc-37007, Santa Cruz Biotechnology, Santa Cruz, CA, USA) in the remaining eye at P12 in a mouse model of OIR. At P17, to validate the knockdown of ORP150, retinal proteins were extracted ($n = 6$ eyes per group) and analyzed by Western blot for ORP150, using rabbit anti-ORP150 (1:1000, Epitomics, Burlingame, CA, USA). Three independent Western blot-based measurements were performed. For quantitative and qualitative assessment of the effect of ORP150 siRNA on neovascularization, at P17, eyes ($n = 12$ eyes per group) were enucleated and fixed in 4%

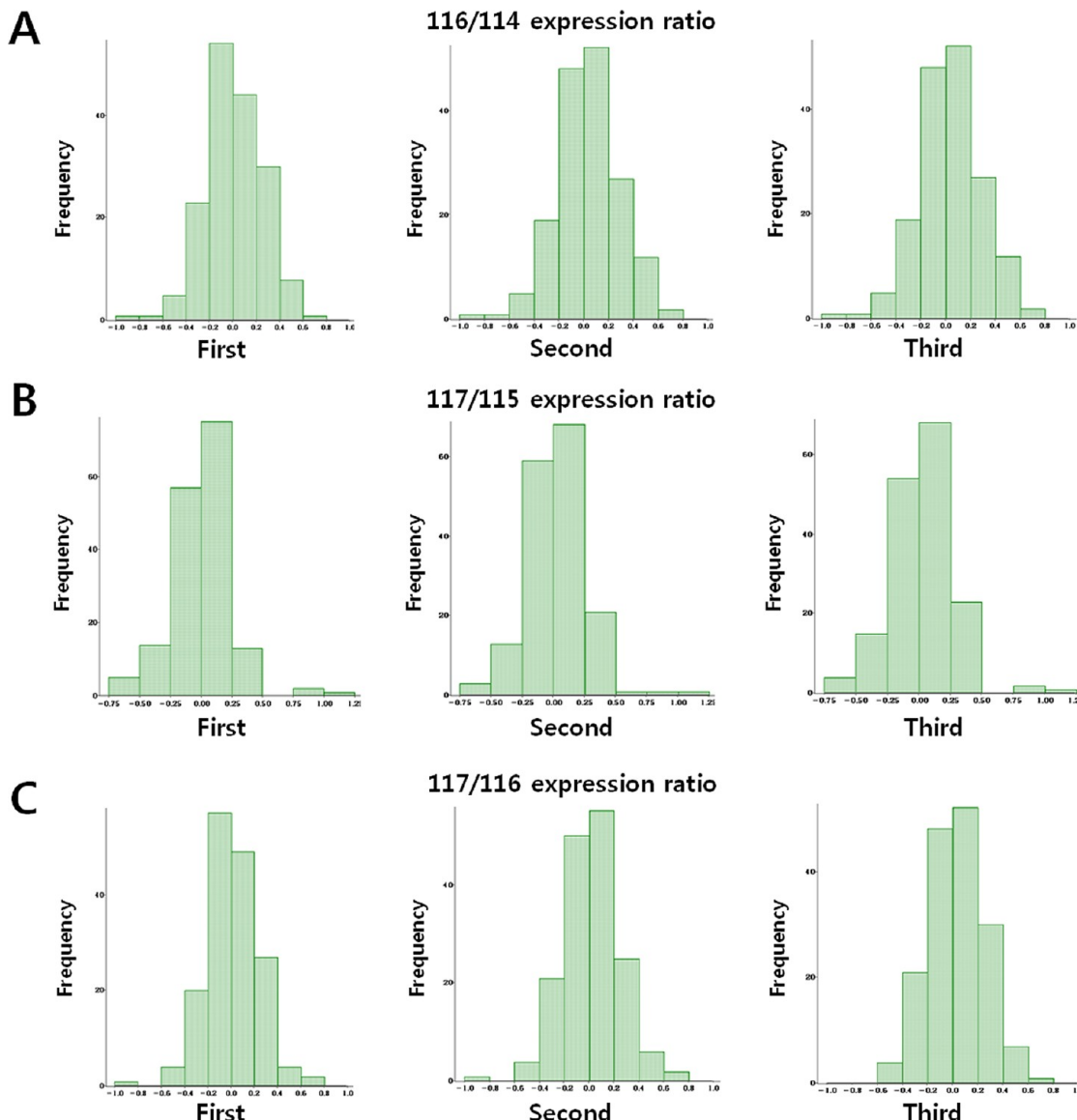


Figure 2. Distribution of \log_2 iTRAQ ratios and determination of cutoff value for significant fold-change. The distribution of \log_2 iTRAQ ratios in (A) postnatal day 12 (P12) versus postnatal day 12 control (P12C), (B) P17 versus P17C, and (C) P17 versus P12 were obtained by comparisons of 3 replicate iTRAQ experiments. All 3 pairwise ratios showed narrow normal distributions, with mean values of 0.019 ± 0.25 , 0.038 ± 0.25 , and 0.038 ± 0.25 in P12 versus P12C; 0.014 ± 0.24 , 0.027 ± 0.23 , and 0.031 ± 0.25 in P17 versus P17C; and 0.017 ± 0.22 , 0.025 ± 0.23 , and 0.022 ± 0.23 in P17 versus P12.

paraformaldehyde. Six eyes per group were embedded in paraffin, and quantitation of neovascularization was performed, as previously described.³¹ In brief, after staining with hematoxylin and eosin, we counted the vascular lumens on the vitreal side of the internal limiting membrane in at least 10 sections from each eye by two independent observers. For qualitative assessment of retinal neovascularization at P17, retinal flat mounts ($n = 6$ eyes per group) were generated. After staining the retinal vessels with TRITC-labeled BS-1 lectin, retinal flat mounts were examined by a confocal microscopy and were compared between ORP150 siRNA treated and control siRNA treated eyes.

In addition, immunofluorescence staining was also performed with primary antibodies against vimentin and glutamine synthetase (Table S1, Supporting Information) to evaluate the changes in Müller glial cells after ORP150 knockdown. Also, density of retinal ganglion cells were determined from the

hematoxylin and eosin stained retinal sections as previously described with some modifications.^{32,33} In brief, photomicrographs were captured at 0.5 and 1.5 mm from the center of the optic nerve head, which represents central avascular retina and peripheral retina with neovascularization, respectively. Cells in the ganglion cell layer were counted by two independent observers and reported as a density of retinal ganglion cells (cells/mm). The values used were averaged from six measurements in each eye.

RESULTS

OIR Mouse Model

The generation of the OIR model was confirmed by histological analysis of the retinal flat mounts and retinal sections. By confocal micrography, flat-mounted retina from the mouse model of OIR showed vaso-obliteration in the central retinal area in the P12 samples and neovascularization in the P17

Table 1. Differentially Expressed Retinal Proteins, as Quantified by iTRAQ at P12 and P17 in OIR^a

Accession No.	Gene name	Protein name	Fold-change		
			P12 : P12C (116 : 114)	P17:P17C (117 : 115)	P17:P12 (117 : 116)
Proteins up- or down-regulated at P12 compared with P12C					
spt Q62188	Dpysl3	Dihydropyrimidinase-related protein	1.72±0.01	1.02±0.01	0.78±0.01
spt P31786	Dbi	Acyl-CoA-binding protein	1.61±0.01	1.48±0.01	0.75±0.01
trm Q8BMU7	Etfα	Electron transfer flavor protein alpha	1.46±0.15	1.28±0.02	0.94±0.02
cra mCP99343	tpm1	tropomyosin 1, alpha	1.45±0.18	1.15±0.09	0.80±0.09
spt P46460	Nsf	Vesicle-fusing ATPase	1.45±0.06	0.90±0.02	0.74±0.03
trm Q9D6A4	Ttr	Putative uncharacterized protein	1.40±0.09	1.10±0.01	0.82±0.01
spt P20443	Sag	S-arrestin	1.37±0.06	1.18±0.02	0.96±0.02
cra mCP114716	Cln5	hypothetical protein	1.33±0.11	1.04±0.01	0.83±0.01
trm Q9Z1R9	Prss1	Trypsinogen 16	1.32±0.02	1.05±0.01	0.75±0.01
trm Q91WE7	Uso1	Vesicle docking protein	1.31±0.01	1.07±0.01	0.82±0.01
cra mCP9707.2	groL1	RIKEN cDNA 2310046H11 gene	1.31±0.01	1.05±0.01	0.71±0.01
spt O88844	Idh1	Isocitrate dehydrogenase [NADP] cytoplasmic	1.30±0.01	1.25±0.04	0.82±0.05
trm Q9DA96	1700016M24Rik	Hypothetical ARM repeat structure-containing protein	1.3±0.03	1.13±0.01	0.71±0.02
trm Q792Y8	Gm10334	Trypsinogen 15	1.28±0.02	0.98±0.01	0.76±0.01
spt P29595	Nedd8	Neddylin	1.28±0.01	1.22±0.01	0.89±0.01
spt P63101	Ywhaz	14-3-3 protein zeta/delta	1.24±0.05	1.20±0.01	0.97±0.02
cra mCP42740.1	pyrE	hypothetical protein	1.23±0.04	1.17±0.01	0.94±0.01
trm Q91XV3	Basp1	22 kDa neuronal tissue-enriched acidic protein	1.23±0.01	1.00±0.01	0.83±0.01
trm Q6NZC5	Ubb	Ubb protein	1.21±0.01	0.88±0.01	0.78±0.01
trm Q8BFZ3	Actbl2	ACTIN, CYTOPLASMIC TYPE 5 homolog	0.80±0.05	0.96±0.02	1.12±0.03
trm Q9CX86	Hnrnpa0	Heterogeneous nuclear ribonucleoprotein A0	0.78±0.01	1.00±0.02	1.20±0.02
rfl NP_034851.1	Lmnb1	lamin B1	0.72±0.02	0.87±0.02	1.14±0.02
pir S04585	Ncam	neural cell adhesion molecule	0.7±0.01	0.71±0.01	1.04±0.01
spt P24547	Impdh2	Inosine-5'-monophosphate dehydrogenase 2	0.51±0.04	1.01±0.01	1.04±0.01
Proteins up- or down-regulated at P17 compared with P17C					
cra mCP74734	Cryba2	crystallin, beta A2	0.73±0.01	2.47±0.01	1.75±0.01
spt P23927	Cryab	Alpha crystallin B chain	1.31±0.03	2.27±0.01	1.00±0.01
pir A39757	Crybb2	beta-crystallin B2	1.02±0.03	1.83±0.03	1.35±0.04
pir CYMSA	Cryaa	alpha-crystallin chain A	1.22±0.03	1.71±0.01	0.90±0.02
spt P07724	Alb	Serum albumin precursor	1.34±0.02	1.50±0.01	1.03±0.02
spt P28352	Apex1	DNA-(apurinic or apyrimidinic site) lyase	1.01±0.01	1.49±0.01	1.13±0.01
spt P17742	Ppia	Peptidyl-prolyl cis-trans isomerase A	1.15±0.06	1.42±0.05	1.1±0.06
trm Q5XJE7	Pgk1	Pgk1 protein	1.13±0.03	1.38±0.01	1.23±0.01
spt P34057	Revrn	Recoverin	1.18±0.01	1.35±0.01	1.12±0.01
spt P40142	Tkt	Transketolase	1.20±0.01	1.31±0.01	1.08±0.01
trm Q8R1P0	Mdh2	Malate dehydrogenase 2, NAD	1.27±0.07	1.30±0.01	0.98±0.01
spt Q04447	Ckb	Creatine kinase, B chain	1.25±0.01	1.27±0.01	0.89±0.01
dbj BAC97894.1	Scrn1	mKIAA0193 protein	0.85±0.01	1.25±0.01	1.23±0.01
cra mCP113378	Ssb	Sjogren syndrome antigen B	0.99±0.03	1.21±0.04	1.13±0.05
cra mCP98175	Vmn1r171	NCAM polypeptide precursor	1.00±0.01	0.82±0.01	0.94±0.01
gb AAH31728.1	Stxbp1	Stxbp1 protein	0.93±0.09	0.80±0.07	1.17±0.07
trm Q91ZZ3	Sncb	Beta-synuclein	0.84±0.03	0.80±0.06	1.09±0.06
spt P30681	Hmgb2	High mobility group protein 2	0.93±0.01	0.80±0.01	0.83±0.01
cra mCP97064	DPYSL3	dihydropyrimidinase-like 3	0.80±0.01	0.8±0.01	1.16±0.01
trm Q80T15	Sle12a5	MKIAA1176 protein	0.88±0.04	0.79±0.02	1.12±0.03
spt P60867	Rps20	40S ribosomal protein S20	0.97±0.01	0.79±0.01	0.83±0.01
trm Q9QZQ8	H2afy	Histone macroH2A1.2 variant (MacroH2A1.2)	0.96±0.05	0.78±0.08	0.91±0.08
spt P43275	Hist1h1a	Histone H1.1 (H1 VAR.3) (H1a)	0.99±0.01	0.74±0.03	0.92±0.04
spt P43274	Hist1h1e	Histone H1.4 (H1 VAR.2) (H1e)	0.97±0.01	0.73±0.01	0.84±0.01
spt P43276	Hist1h1b	Histone H1.5 (H1 VAR.5) (H1b)	0.92±0.04	0.68±0.01	0.84±0.01
rfl NP_056601.1	Hist1h1c	histone 1, H1c	0.88±0.01	0.66±0.01	0.82±0.02
spt P56564	Slc1a3	Excitatory amino acid transporter 1	0.71±0.01	0.64±0.01	1.15±0.01
cra mCP51905	MCA1905	Core histone H2A/H2B/H3/H4	0.74±0.01	0.63±0.01	0.90±0.01
trm Q64478	Hist1h2bh	Histone H2b (Histone protein Hist1h2bh)	0.73±0.01	0.57±0.01	0.86±0.01

Table 1. continued

Accession No.	Gene name	Protein name	Fold-change		
			P12 : P12C (116 : 114)	P17:P17C (117 : 115)	P17:P12 (117 : 116)
Proteins up- or down- regulated at P17 compared with P12					
rf XP_483976.1	Gapdh	similar to glyceraldehyde-3-phosphate dehydrogenase	0.64±0.05	1.06±0.08	1.62±0.08
trm Q9CY54	Hbb-b1	Hemoglobin, beta adult major chain	0.93±0.02	1.33±0.07	1.56±0.08
crajm CP51933.1	eno1	microtubule-associated protein 1 B	0.82±0.01	1.41±0.01	1.55±0.01
crajm CP10468.2	Dnmt3b	aldolase 1, A isoform	0.95±0.01	1.19±0.02	1.42±0.02
spt P35564	Canx	Calnexin precursor	0.72±0.01	0.92±0.10	1.39±0.10
trm Q80WM3	Cplx4	Complexin IV	0.85±0.01	0.92±0.06	1.38±0.07
rf XP_484728.1	Eno1	similar to Eno1 protein	0.96±0.01	1.14±0.02	1.34±0.02
rf XP_134169.2	Slc25a4	solute carrier family 25	0.83±0.03	0.85±0.01	1.33±0.01
spt Q60932	Vdac1	Voltage-dependent anion-selective channel protein 1	0.95±0.02	0.99±0.01	1.32±0.01
rf XP_486749.1	Gapdh	similar to glyceraldehyde-3-phosphatedehydrogenase	1.14±0.07	1.12±0.14	1.27±0.15
spt P46096	Syt1	Synaptotagmin-1	0.84±0.02	0.85±0.04	1.27±0.04
spt P18572	Bsg	Basigin precursor	0.89±0.01	1.24±0.02	1.27±0.03
trm Q6P5D0	Dpysl2	Dihydropyrimidinase-like 2	0.95±0.04	1.16±0.03	1.25±0.04
spt P20152	Vim	Vimentin	0.99±0.02	1.16±0.02	1.25±0.03
spt P16125	Ldhb	L-lactate dehydrogenase B chain	0.82±0.09	1.07±0.12	1.22±0.13
spt Q61696	Hspal1a	Heat shock 70 kDa protein 1A	0.87±0.02	0.98±0.03	1.22±0.03
rf NP_035229.2	Pkm2	pyruvate kinase 3	0.96±0.01	1.06±0.01	1.21±0.01
trm Q99JF8	Psip1	Lens epithelium-derived growth factor a	1.02±0.01	0.84±0.02	0.79±0.03
spt P09602	Hmgn2	Nonhistone chromosomal protein HMG-17	1.44±0.04	0.79±0.02	0.52±0.03

^aValues were derived from a pooled sample of OIR retinas, and the iTRAQ experiment was performed in triplicate. Proteins were grouped according to the day that had the greatest upregulation or downregulation relative to each control. Increases in expression are marked in red, and decreases are shown in blue.

samples (Figure 1). Additionally, neovascular tufts on the vitreal side of the internal limiting membrane were observed in P17 samples, in contrast to the normal retinal vasculature of the P17 control (Figure 1).

Identification of Differential Proteomes Using iTRAQ

We identified 699 proteins from 2437 peptides in the 3 combined iTRAQ experiments at a minimum confidence level of 95% (unused ProtScore >1.3) (Figure S1, Supporting Information). The detailed protein identification data are listed in Table S2, Supporting Information. Of the proteins that were identified by iTRAQ, 54% comprised 1-peptide proteins, 15% was a 2-peptide protein, 8% was a 3-peptide protein, 4% was a 4-peptide protein, and 19% comprised proteins with 5 or more peptides (Figure S1, Supporting Information). 182 proteins (unused ProtScore >1.3) were common to all 3 iTRAQ experiments at a minimum confidence level of 95% using 3 pooled retina samples.

To analyze the functional annotation of the identified retinal proteome, the 699 proteins were classified into “molecular function” subcategories using the PANTHER classification program, shown in Figure S2, Supporting Information. The 2 largest components, “nucleic acid-binding” proteins and “cytoskeletal proteins”, constituted 24 and 10%, respectively, of the 699 proteins (Figure S2, Supporting Information).

Determination of the Cutoff Threshold for Significant Fold-Changes in the iTRAQ Experiments

In the LC–MS/MS experiments using iTRAQ labeling, the labeling efficiency was examined as described, wherein the total number of possible labeling sites (lysine side chains and N-termini of all peptides) for the iTRAQ tags were compared with those of the detected peptides.^{25,26} The labeling efficiency was greater than 98% in these iTRAQ experiments (data not shown).

To obtain bona fide iTRAQ results, possible variations in the replicate iTRAQ experiments must be identified and minimized. In calculating the cutoff threshold for meaningful fold-changes over experimental errors, the variations between experimental replicates were considered to be actual variations in the 3 iTRAQ experiments. Consequently, the 3 iTRAQ experiments identified 699 proteins, but the number of commonly identified proteins was 182.

Using the following selection criteria, containing more than 2 unique peptides (>95%), a *p*-value < 0.05, and error factor (EF) < 2, in the P12 versus P12C, P17 versus P17C, and P12 versus P17 OIR tissue comparisons, 165 proteins were quantitated in the 3 iTRAQ experiments. These proteins were used initially to determine the experimental variations and confirm the cutoff threshold for meaningful fold-changes.³⁴ As shown in Figure 2A, the 3 pairwise ratios of P12 versus P12C had a narrow normal distribution, with mean values of 0.019 ± 0.25 , 0.038 ± 0.25 , and 0.038 ± 0.25 (95% confidence interval), consistent with an expected ratio of 1.0 and a relative standard deviation (SD) of 17.7–18.5% on a linear scale.

For P17 versus P17C, the pairwise ratios also exhibited a narrow normal distribution, with mean values of 0.014 ± 0.24 , 0.027 ± 0.23 , and 0.031 ± 0.25 (95% confidence interval), consistent with an expected ratio of 1.0 and a relative SD of 18.2–19.7% on a linear scale. The pairwise ratios of P12 versus P17 assumed a narrow normal distribution, with mean values of 0.017 ± 0.22 , 0.025 ± 0.23 , and 0.022 ± 0.23 (95% confidence interval), consistent with an expected ratio of 1.0 and a relative SD of 16.0–16.6% on a linear scale.²⁹

On the basis of the 3-standard deviation model, we concluded that a fold-change of >1.20 or <0.83 was a meaningful cutoff that reflected actual differences in protein expression between the 116/114, 117/115, and 117/116 reporter ions. Ultimately, 72 proteins had a *p*-value < 0.05, EF < 2, more than 2 unique peptides with >95% confidence

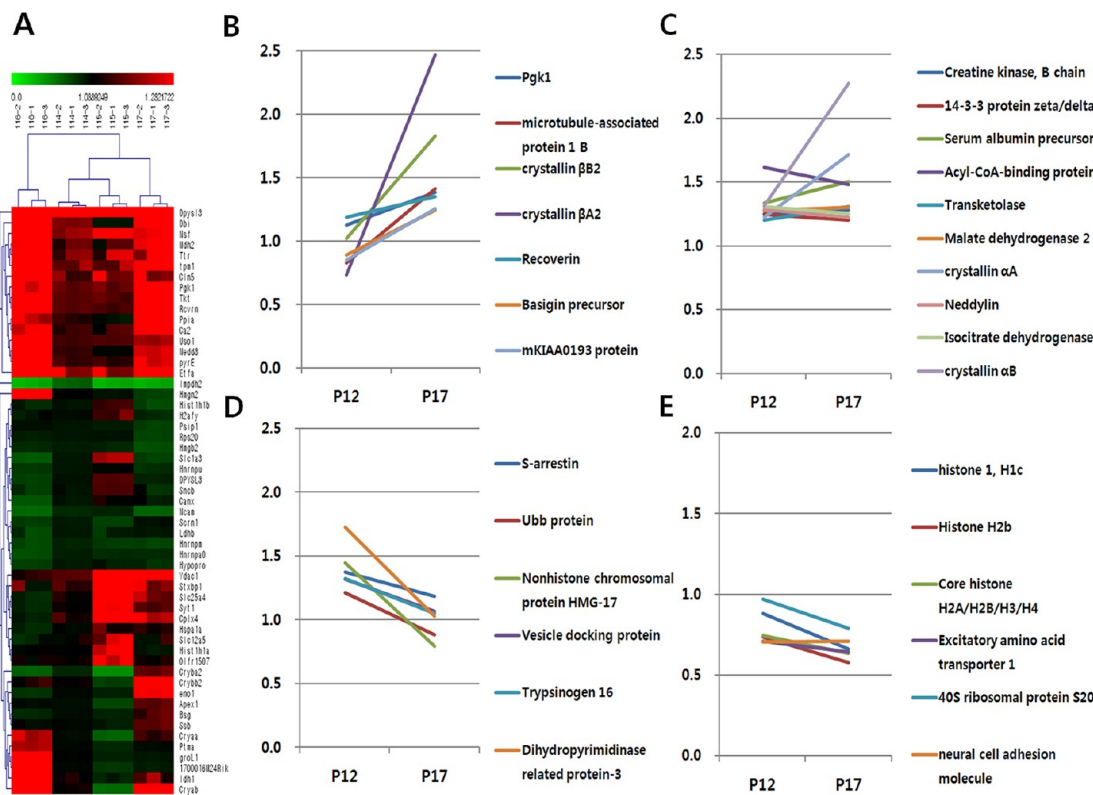


Figure 3. Cluster analysis of differentially expressed proteins in P12 and P17 retinas. (A) Hierarchical clustering (HLC) was performed using MultiExperiment Viewer (Version 4.3), on the basis of the average area values for differentially expressed proteins from the iTRAQ experiments. The specific expression patterns were obtained by subclustering analysis, wherein 4 subclusters were analyzed: 1 (upregulated in P17, B), 2 (upregulated in both P12 and P17, C), 3 (upregulated in P12, D), and 4 (downregulated in P17, E). Y-axis, fold change compared to each control.

level, and expression that modulated by $> \pm 1.20$ -fold in all 3 iTRAQ experiments (Table S3, Supporting Information).

Differential Proteomes of P12 of OIR

Of the 72 quantified proteins from the iTRAQ experiment, 39 proteins were differentially expressed in P12 retinas (116 reporter) compared with P12C (114 reporter), comprising 25 upregulated and 14 downregulated proteins (Table 1 and Table S3, Supporting Information).

The 72 quantified proteins from the iTRAQ experiment were classified into “biological processes” using the PANTHER classification program. The biological process subcategories for the selected differentially expressed proteins are summarized in Table S3, Supporting Information. With regard to “biological process” subcategories for P12, “carbohydrate metabolism” (75%), “protein metabolism” (83%), and “signal transduction” (50%) were upregulated compared with P12C (Figure S3A and Table S3, Supporting Information). In contrast, “cell structure and motility” (75%), “nucleotide metabolism” (92%), and “signal transduction” (50%) were downregulated (Figure S3A and Table S3, Supporting Information).

Differential Proteomes of P17 of OIR

In the P17 retinas (117 reporter), 38 differentially expressed proteins (21 upregulated and 17 downregulated) were identified versus P17C (115 reporter) (Table 1 and Table S3, Supporting Information).

In the “biological process” subcategories for P17, “carbohydrate metabolism” (100%), “cell structure and motility” (100%), and “signal transduction” (100%) were upregulated compared with P17C (Figure S3B and Table S3, Supporting Information), and “nucleotide metabolism” (86%) and “protein

metabolism” (25%) were downregulated (Figure S3 and Table S3, Supporting Information).

Comparison of Proteomes between Hyperoxic (P12) and Hypoxic Retinas (P17)

On comparison of the P17 and P12 proteomes, 36 differentially expressed proteins (21 upregulated and 15 downregulated) were identified in P17 retinas (Table 1 and Table S3, Supporting Information).

In the “biological process” subcategories for P17, “nucleotide metabolism” (73%) and “protein metabolism” (71%) were downregulated versus P12 (Figure S3C and Table S3, Supporting Information), and “carbohydrate metabolism” (88%), “cell structure and motility” (67%), and “signal transduction” (100%) were upregulated (Figure S3 and Table S3, Supporting Information).

Cluster Analysis of Differentially Expressed Proteomes

Next, we analyzed the protein expression patterns over time, on the basis of rises and declines in protein levels at P12 and P17: the hyperoxic and hypoxic phases, respectively. For the cluster analysis of differentially expressed proteins in the OIR-induced model, MultiExperiment Viewer (<http://mev.tm4.org>, Version 4.3) was used to determine the proteins or pathways that are involved in the pathogenesis of OIR. HLC was performed for the 72 differentially expressed proteins in P12C, P17C, P12, and P17 retinas, on the basis of one-way clustering methods (Figure 3A). In the hierarchical clustering, the P12C (114 reporter) and P17C (116 reporter) retinal proteomes had similar expression patterns, whereas the P12 (116 reporter) and P17 (117 reporter) proteomes had disparate patterns versus the P12C and P17C proteomes, respectively (Figure 3A).

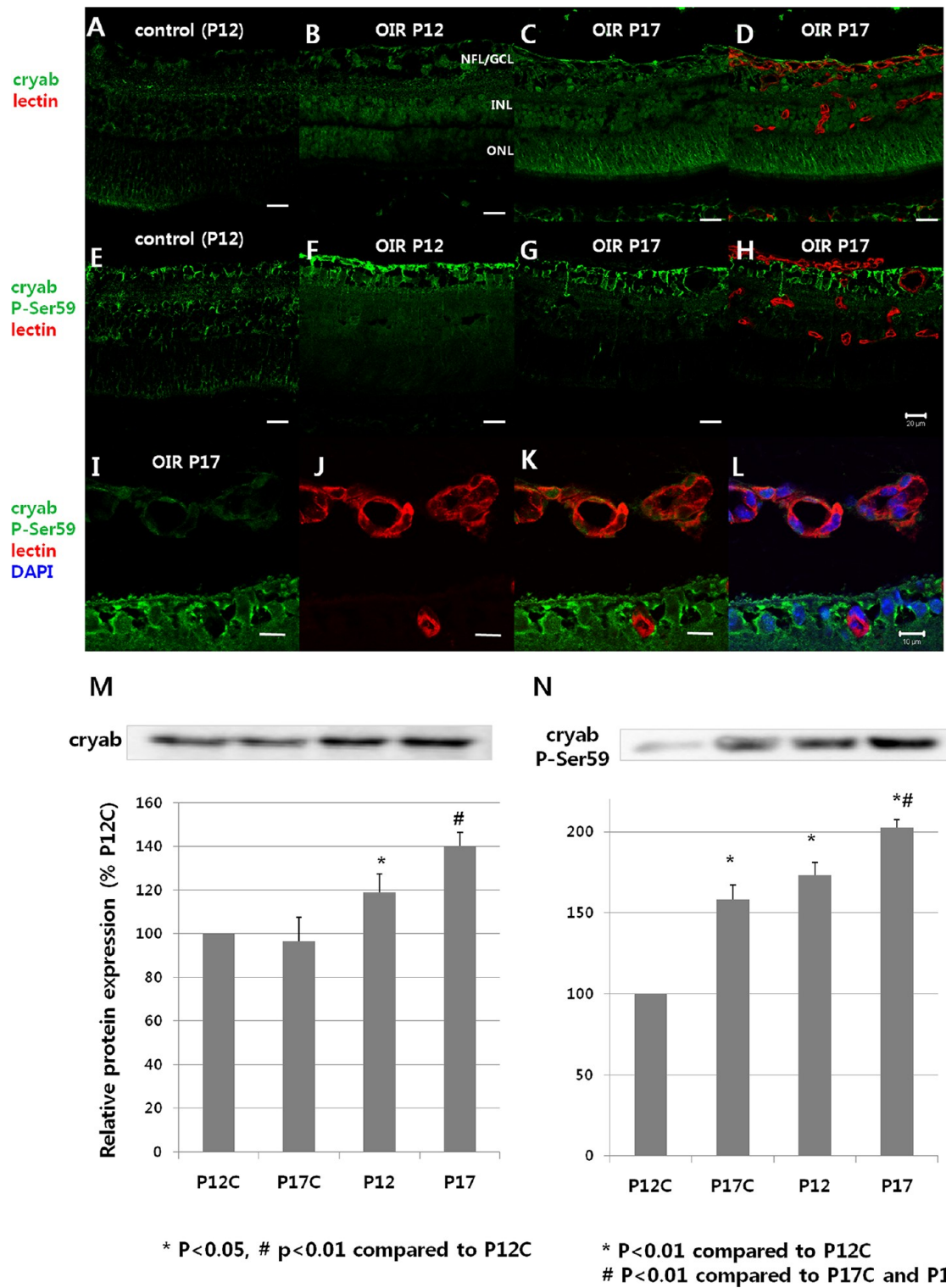


Figure 4. Immunolocalization and Western blot analysis of Crystallin α B in oxygen-induced retinopathy (OIR). In control retinas, positive immunoreactivity for Crystallin α B (green) was observed in the ganglion cell layer/nerve fiber layer (GCL/NFL), inner plexiform layer (IPL), inner nuclear layer (INL), and outer nuclear layer (ONL) (A). In OIR postnatal day 12 (P12) and P17 retinas, the immunoreactivity for Crystallin α B was increased (B–D). In OIR P17 retinas, the signal intensity was increased in the inner retinal surface and ONL (C, D). In OIR P12 and P17 retinas, the immunoreactivity for Crystallin α B P-Ser-59 (green) was intense in the GCL/NFL compared with control (E–H). In OIR P17 retinas, higher-magnification images of double-immunolabeling of Crystallin α B P-Ser-59 with BS-1 lectin (red) showed positive but weaker immunoreactivity of neovascular tufts versus the GCL/NFL (I–L). By Western blot, retinal expression of Crystallin α B and Crystallin α B P-Ser-59 was significantly up-regulated in P12 and P17, compared with that of the control retinas (M, N). In OIR P17 retinas, the expression of Crystallin α B P-Ser-59 was more up-regulated, compared with OIR P12 retinas (N). Data are the means \pm SEM of the three independent Western blot-based measurements. Scale bar: (A–H), 20 μ m; (I–L), 10 μ m. Blue, DAPI.

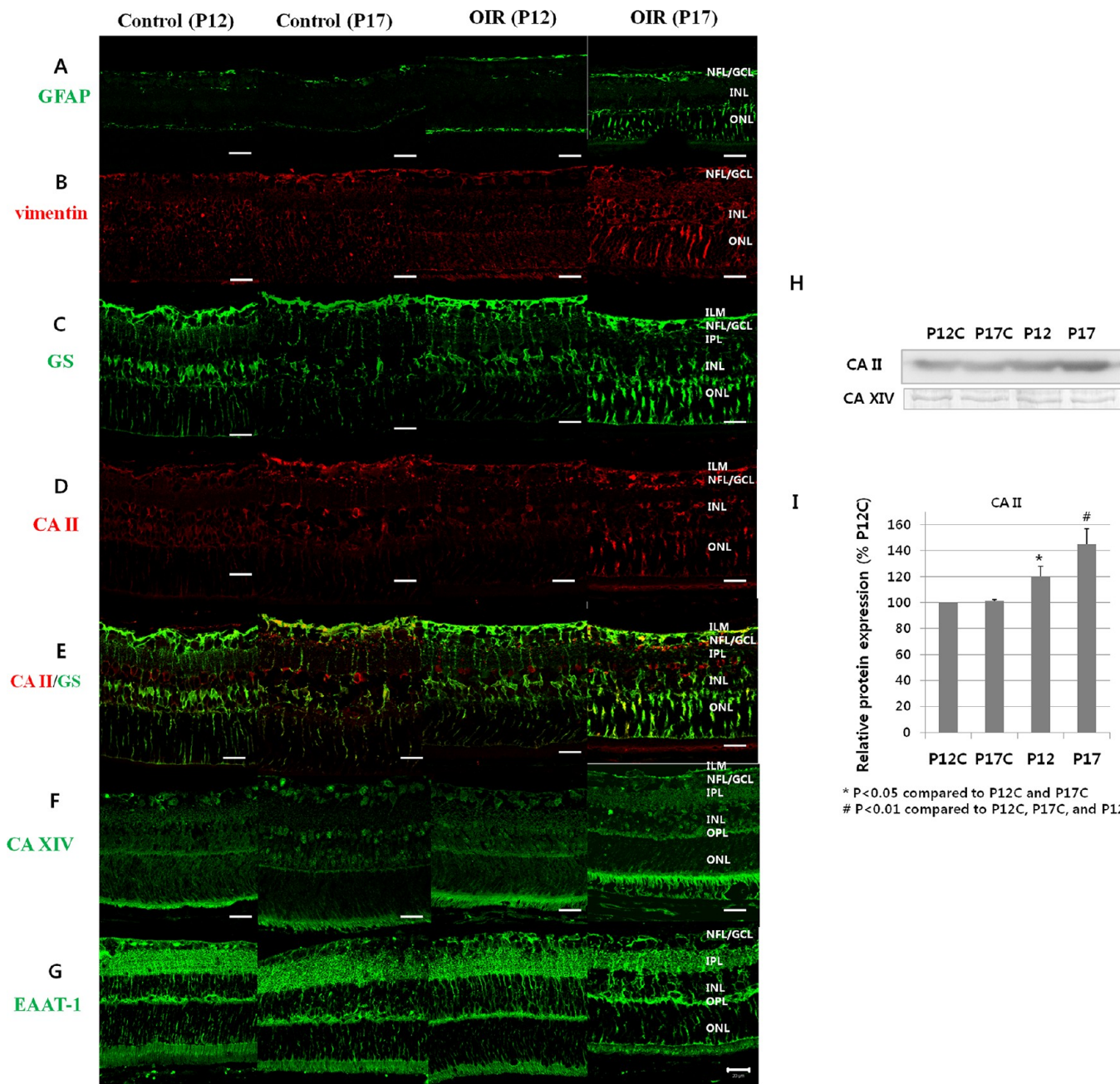


Figure 5. Immunolocalization of proteins expressed primarily in Müller cells. In oxygen-induced retinopathy (OIR) postnatal day 17 (P17) retinas, the immunoreactivity for glial fibrillary acidic protein (GFAP), vimentin, and glutamine synthetase (GS) was increased compared with the control and OIR P12 retinas, especially in the distal branches of the Müller cells (A–C). The retinal expression of carbonic anhydrase II (CA II), which was colocalized with GS, increased in OIR P17 retinas (D, E). Quantitation of CA II by Western blot showed that CA II was significantly up-regulated in the OIR P17 retina than in the control retinas (H, I). Also, CA II in the OIR P17 retina was more up-regulated than in the OIR P12 and normal control retinas (H, I). Data are the means \pm SEM of the three independent Western blot-based measurements (I). In contrast, the immunoreactivity for CA XIV in the Müller cells was not changed (F), and the Western blot for CA XIV showed no difference between the OIR and control (H). Positive immunoreactivity for excitatory amino acid transporter 1 (EAAT-1) was observed in all retinal layers, without apparent differences between OIR and control retinas (G). P12C and P17C, control eyes enucleated on P12 and P17, respectively. Scale bar: 20 μ m. NFL/GCL, nerve fiber layer/ganglion cell layer; INL, inner nuclear layer; ONL, outer nuclear layer.

In the subclustering analysis, we categorized major patterns of up- and downregulation into 4 subclusters: subclusters 1 (upregulated in P17), 2 (upregulated in P12 and P17), 3 (upregulated in P12), and 4 (downregulated in P17).

Subcluster 1 was composed of 7 proteins (phosphoglycerate kinase 1 (PGK1), microtubule-associated protein 1 B (MAP1B), Crystallin β A2, Crystallin β B2, recoverin, basigin

precursor, and mKIAA0193) that were upregulated in P17 (Figure 3B).

Subcluster 2 comprised 10 proteins (creatine kinase B, 14-3-3 protein zeta/delta, serum albumin precursor, acyl-CoA-binding protein, transketolase, malate dehydrogenase 2, Crystallin α A, neddylin, isocitrate dehydrogenase, and Crystallin α B) that rose in expression in P12 and P17 (Figure 3C).

Subcluster 3 contained 6 proteins (s-arrestin, UbB protein, nonhistone chromosomal protein HMG-17, vesicle-docking protein, trypsinogen 16, and dihydropyrimidinase-related protein-3) that were upregulated in P12 but downregulated in P17 retinal tissue (Figure 3D).

Subcluster 4 comprised 6 proteins (histone 1, histone H2b, NRAA, excitatory amino acid transporter 1, 40S ribosomal protein, and neural cell adhesion molecule) that were downregulated in P17 retinal tissue (Figure 3E).

Identified Proteins from LC-MS/MS Analysis Using LTQ Velos

To identify specific proteins in P12 and P17 OIR tissue, we used a complementary LC-ESI-MS/MS analytical platform with LTQ Velos. In total, 1074 retinal proteins were identified in P12C, P17C, P12, and P17 retinal tissue (Figure S4A and Table S4, Supporting Information); 364 proteins were common between P12C and P12 retinal tissue, and 34 and 578 proteins were unique in P12C and P12 retinas, respectively (Figure S4B, Supporting Information). 496 proteins were common between P17C and P17 retinal tissue, and 270 and 135 proteins, respectively, were unique (Figure S4C, Supporting Information). Forty-three and 138 proteins were unique in P17 and P12 retinas, respectively (Figure S4A and Table S4, Supporting Information).

In this LC-ESI-MS/MS analysis, 723 proteins were newly identified compared with the iTRAQ results. Thus, 1422 proteins were identified using iTRAQ and the LTQ Velos (Figure S4D, Supporting Information).

Selection of Proteins of Interest

The nano-LC-ESI-MS/MS and iTRAQ experiment of OIR retinal tissue implicated certain changes in the retinal proteome as therapeutic targets for further study with regard to their function in angiogenesis, vascular changes, and neurodegeneration. Five proteins (Crystallin α A, Crystallin α B, PGK1, lens epithelium-derived growth factor (LEDGF/Psip1), and excitatory amino acid transporter 1 (Slc1a3/EAAT-1/GLAST)) were selected by iTRAQ, and 3 proteins (CA II, CA XIV, and crystalline β S) were selected by LTQ analysis. To examine their localization in the OIR retina, we examined retinal sections from control and OIR retinas by immunohistochemistry.

Retinal Expression of Crystallin α A, α B, and β S

The nano-LC-ESI-MS/MS and iTRAQ experiments identified Crystallin α A and α B in control and OIR retinas. The iTRAQ experiments demonstrated that Crystallin α A and α B were upregulated to a greater extent in OIR P17 than in OIR P12 retinas. Crystallin α A was immunoreactive in all retinal layers in control and OIR retinas, throughout the Müller cells (Figure S5, Supporting Information). In OIR P17 retinas, there was intense immunoreactivity of Crystallin α A in the ganglion cell layer (GCL) and inner nuclear layer (INL) (Figure S5, Supporting Information).

Positive immunoreactivity for Crystallin α B was observed in the ganglion cell layer/nerve fiber layer (GCL/NFL), inner plexiform layer (IPL), INL, and outer nuclear layer (ONL) in control retinas (Figure 4). In OIR P12 and P17 retinas, Crystallin α B immunoreactivity increased in all retinal layers (Figure 4). In OIR P17 retinas, the signal intensity rose, especially in the inner retinal surface and ONL. By Western blot, retinal expression of Crystallin α B was significantly upregulated in P12 and P17, compared with the control retinas (Figure 4).

The chaperone activity of Crystallin α B is regulated by its phosphorylation, particularly at Ser59.³⁵ In OIR P12 and P17 retinas, the immunoreactivity of Crystallin α B P-Ser-59 was robust in the GCL/NFL (Figure 4). Higher-magnification images of double immunolabeling of Crystallin α B P-Ser-59 with TRITC-labeled BS-1 lectin showed double-positive but weaker immunoreactivity in the neovascular tufts than in the GCL/NFL. By Western blot, the retinal expression of Crystallin α B P-Ser-59 was also significantly up-regulated in P12 and P17, compared with the control retinas (Figure 4).

Crystallin β S was identified by nano-LC-ESI-MS/MS in all 4 groups (Table S3, Supporting Information). In the retinal sections, Crystallin β S immunoreactivity rose in the ONL of P12 and P17 OIR retinas (Figure S5, Supporting Information).

Retinal Expression of Proteins Predominantly in Müller Glial Cells

Retinal expression of glial fibrillary acidic protein (GFAP), a marker for astrocytes and activated Müller glial cells, increased in OIR P17 retinas (Figure 5). Additionally, immunoreactivity for vimentin and glutamine synthetase, markers of Müller cell gliosis, rose in the distal branches of Müller cells in OIR P17 retinas compared with control and OIR P12 retinas (Figure 5).

Nano-LC-ESI-MS/MS identified CA II and CA XIV, 2 isoenzymes of CA, in the retina.³⁶ To measure the retinal expression of CA II and CA XIV, we performed Western blot and immunohistochemistry. Quantitation of CA II by Western blot showed that CA II was significantly up-regulated in the OIR P12 retina than in the control retinas at P12 and P17 (Figure 5). Also, CA II in the OIR P17 retina was more up-regulated than in the OIR P12 retina and normal control retinas (Figure 5). At P17, retinal CA II expression increased in the NFL/GCL, INL, and ONL, colocalizing with markers of Müller glial cells, such as glutamine synthetase (Figure 5) and vimentin (Figure S6, Supporting Information). CA II immunoreactivity was prominent in the distal branches of Müller cells on P17. In contrast to CA II, there was no difference in CA XIV expression by Western blot between OIR and control tissues (Figure 5). CA XIV was immunoreactive in all retinal layers, especially in the internal limiting membrane (ILM), outer plexiform layer (OPL), the inner aspect of the subretinal space, and the RPE layer, with similar patterns in all groups (Figure 5).

In the iTRAQ experiment, EAAT-1, a major glutamate transporter of Müller glial cells, was downregulated in OIR P12 and P17 retinas (Table S3, Supporting Information, Figure 3B). Positive immunoreactivity for EAAT-1 was observed in all retinal layers, particularly the IPL and OPL, but there was no difference between OIR and control retinas (Figure 5).

Retinal Expression of PGK1 and ORP150

In the iTRAQ experiment, PGK1 was upregulated in OIR P17 retinas compared with OIR P12 and control P17 retinas (Table S3, Supporting Information, Figure 3B). PGK1 was immunoreactive in all retinal layers and colocalized with the neovascular tufts (Figure S7, Supporting Information).

By nano-LC-ESI-MS/MS, ORP150 was expressed in OIR P12 and P17 retinas. Additionally, in the iTRAQ experiment, ORP150 appears in all 4 groups with 1 identified peptide. Although only 1 peptide was identified, ORP150 levels increased greater than 1.4-fold by iTRAQ in P12 and P17 compared with P12C and P17C, respectively.

Quantitation of ORP150 by Western blot showed that ORP150 was significantly up-regulated in OIR P12 and P17

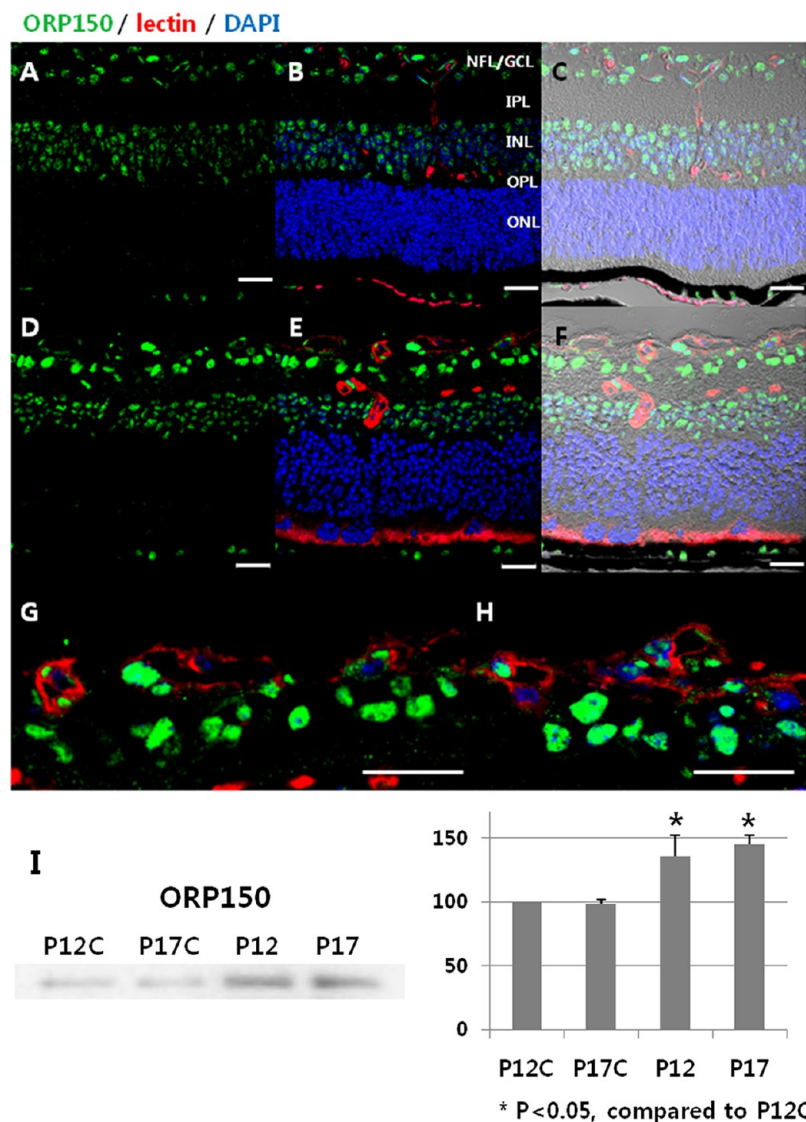


Figure 6. Immunolocalization of 150-kDa oxygen-regulated protein 150 (ORP150) in oxygen-induced retinopathy (OIR). In the retinal section, immunoreactivity for ORP150 (green) was detected in the perinuclear region of the ganglion cell layer, the inner nuclear layer, and the retinal pigment epithelium layer in control (A, B, C) and OIR postnatal day 17 (P17) retinas (D, E, F). In OIR P17 retinas, ORP150 colocalized with the neovascular tufts but not with the intraretinal vasculature (G, H). Quantitation of ORP150 by Western blot showed that ORP150 was significantly up-regulated in OIR P12 and P17 retinas, compared with that of the control retinas at P12 and P17 (I). Data are the means \pm SEM of the three independent Western blot-based measurements. NFL/GCL, nerve fiber layer/ganglion cell layer; IPL, inner plexiform layer; INL, inner nuclear layer; OPL, outer plexiform layer; ONL, outer nuclear layer. Scale bar: 20 μ m.

retinas, compared with that of the control retinas at P12 and P17 (Figure 6). In the retinal sections, ORP150 immunoreactivity was detected in the perinuclear region of the GCL, INL, and RPE layer (Figure 6). Notably, in OIR P17 retinas, ORP150 immunoreactivity was intense in the inner retinal layers and colocalized with the neovascular tufts (Figure 6). ORP150 immunoreactivity was not colocalized with immunoreactivity of Iba-1, a microglial marker (Figure S8, Supporting Information).

Retinal Expression of LEDGF

In the iTRAQ experiment, LEDGF was downregulated in P17 compared with P12 (Table S3, Supporting Information). LEDGF was immunoreactive in all retinal nuclear layers but did not differ between groups (Figure S5, Supporting Information).

Function of ORP150 in VEGF Secretion in Retinal Pigment Epithelium

To examine the function of ORP150 in retinal angiogenesis, the secretion of VEGF by retinal pigment epithelium (RPE) cells was measured after downregulation of ORP150 expression. By Western blot, ORP150 expression declined on transfection with ORP150 siRNA (Figure 7A). Further, secreted VEGF levels by ARPE-19 cells fell significantly 24 h after transfection ($P < 0.01$, t test) (Figure 7B).

Effect of siRNA Targeting ORP150 on Retinal Neovascularization in OIR

Quantitation of ORP150 by Western blot showed that intravitreally administered siRNA targeting ORP150 substantially down-regulated the retinal expression of ORP150 (Figure 8). Both qualitative and quantitative assessment of the retinal neovascularization showed that the intravitreally administered

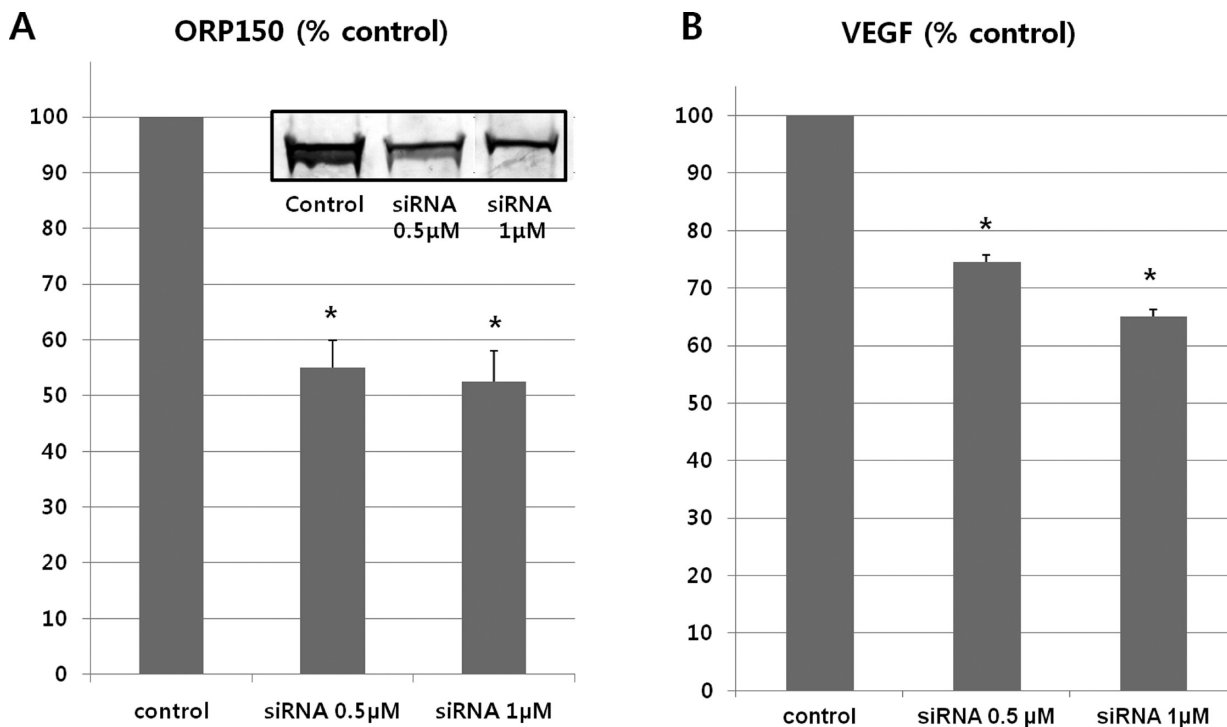


Figure 7. Effect of 150-kDa oxygen-regulated protein (ORP150) knockdown by siRNA on vascular endothelial growth factor (VEGF) secretions in retinal pigment epithelium. Analysis of protein knockdown in ARPE-19 cells 24 h after transfection with ORP150 siRNA (A). The graph was generated from densitometric scans of gel bands of a Western blot. Additionally, ARPE-19 cell-secreted VEGF was measured by ELISA and decreased significantly 24 h after transfection (B). Data are the means \pm SEM of the three independent experiments. * $P < 0.01$ vs control. The value of the control was set to 100%.

siRNA targeting ORP150 significantly reduced the retinal neovascularization in a mouse model of OIR (Figure 8). We also investigated whether the antiangiogenic effect was associated with Müller cell activation. However, immunoreactivity for vimentin and glutamine synthetase, markers for Müller cell gliosis, was not different between ORP150 siRNA-treated retina and control siRNA-treated retina (Figure S9, Supporting Information). Further, to investigate whether the antiangiogenic effect of siRNA targeting ORP150 was associated with degeneration of retinal ganglion cells, density of retinal ganglion cells were determined. In hematoxylin and eosin stained retinal sections, densities of retinal ganglion cells at 0.5 and 1.5 mm from the center of the optic nerve head showed no statistically significant difference between control and ORP150 siRNA injected eyes ($P > 0.05$, Figure S10, Supporting Information).

■ DISCUSSION

In this study, the nano-LC-ESI-MS/MS and iTRAQ experiment generated 1422 retinal proteins in the mouse model of OIR and in normally developing mice. Of the differentially expressed proteins between control and OIR retinas, we identified several targets for further study with regard to their function in angiogenesis, vascular change, and neuronal dysfunction in ischemic retinopathy. A comprehensive proteome profile of the developing mouse retina was also acquired in this study. Moreover, proteins of interest, including the Crystallin family, CA II and CA XIV, EAAT-1, LEDGF, PGK1, and ORP150, were characterized.

We observed that Crystallin proteins, including Crystallin α A, α B, β A2, β B2, and β S, were upregulated in OIR retinas. Previous reports have demonstrated upregulation of Crystallin

α B in OIR,³⁷ but our findings of upregulation of other Crystallin family members in OIR are novel.

Retinal expression of Crystallin α A and α B, which belong to the small heat shock protein family, increases by light damage, retinal trauma, and diabetes and declines with optic nerve injuries.^{38–40} The overexpression of Crystallin α A and α B has neuroprotective effects on retinal ganglion cells.⁴¹ In our study, the increased expression of Crystallin α A and α B in ganglion cell layers might also constitute a neuroprotective mechanism in OIR. Kase et al.³⁷ demonstrated that Crystallin α B functions as a chaperone for VEGF-A during retinal angiogenesis. In our study, Crystallin α B P-Ser-59 immunoreactivity was robust in the GCL/NFL in P12 and P17 retinas, consistent with Kase et al.³⁷ However, the immunoreactivity was less intense in the neovascular tufts than in the GCL/NFL in P17, suggesting that the activity of Crystallin α B as a chaperone for VEGF-A is more prominent in the inner retinal tissue than in neovascular tufts.

Retinal expression of Crystallin β A2 and β B2 increases in animal models of diabetes and ocular hypertension-induced ganglion cell death.^{18,42} In addition, Crystallin β B2, expressed primarily in retinal ganglion cells, promotes axonal regeneration.⁴³ In the OIR model, neuronal dysfunction of the rod and cone, with altered macro- and microglial activity, occurs.¹² Increased beta-Crystallin levels might be a neuroprotective mechanism. Crystallin β S, also known as Crystallin γ S, was upregulated in the outer retinal layer in OIR. Similar to α -crystallins, Crystallin β S might be a stress-induced protein, a subfamily of heat-shock proteins with low molecular weights.⁴⁴ Despite their implication in several retinal diseases, the function of Crystallin family members, other than Crystallin α B in OIR, is unknown.

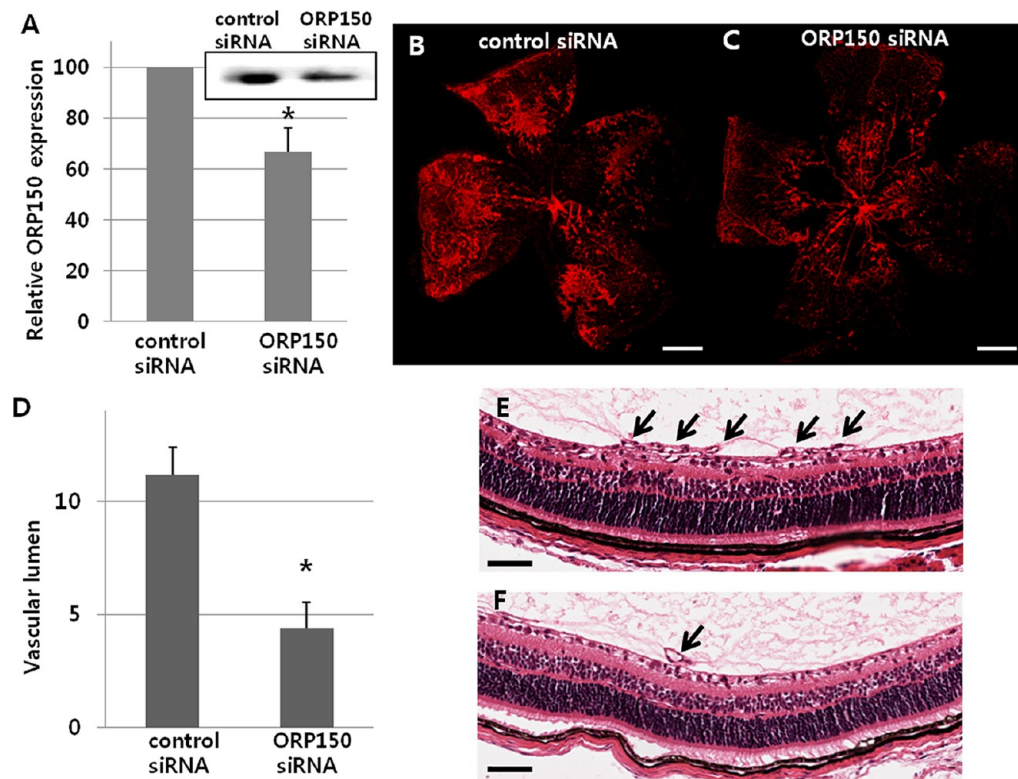


Figure 8. The effect of siRNA targeting 150-kDa oxygen-regulated protein (ORP150) on retinal neovascularization in OIR. Quantitation of ORP150 by Western blot showed that intravitreally administered siRNA targeting ORP150 significantly down-regulated retinal expression of ORP150 (A). Data are the means \pm SEM of three independent Western blot-based measurements. Compared to the control siRNA-treated retina (B), less retinal neovascularization on retinal flat mounts was observed in siRNA targeting ORP150 treated retina (C). Quantitative assessment of retinal neovascularization was done by counting the vascular lumens (arrows) on the vitreal side of the inner limiting membrane (D, E, F). The average lumens per section for each group ($n = 6$ eyes each) are presented as the means \pm SEM. Note that there is a significant difference in the retinal neovascularization between the control and ORP150 siRNA treated eyes (* $P < 0.05$). Scale bar: 500 μ m (B, C), 50 μ m (E, F).

In our study, we identified proteins that were expressed primarily in Müller cells, including glutamine synthetase, GFAP, vimentin, CA II, and EAAT-1. Glutamine synthetase, a marker for specific Müller cell gliosis, in addition to GFAP and vimentin, markers for nonspecific gliosis, was upregulated, especially in the distal branches of Müller cells.^{45,46} Reactive gliosis of Müller cells, in response to nearly any pathological change in the retina, has cytoprotective and cytotoxic effects on the retina.^{45,46} That several markers of gliosis were upregulated in OIR highlights the significance of Müller cell gliosis during the development of ischemic retinopathy.

In addition, the expression of CA II and XIV, 2 isoforms of CA in the neural retina, has been examined.⁴⁷ In the retina, CA has a significant function in pH regulation, fluid absorption, and retinal vascular permeability.³⁶ In our study, the retinal expression of CA II, a cytoplasmic protein, increased in OIR and colocalized with vimentin and glutamine synthetase. In contrast, immunoreactivity for CA XIV, a membrane-bound protein that is expressed primarily in Müller cells in addition to in RPE, was unchanged in OIR.⁴⁸ CAII is elevated in the vitreous of eyes with diabetic retinopathy and raises retinal vascular permeability;²⁰ i.e., CAII is selectively upregulated in Müller cell gliosis and might contribute to increased retinal vascular permeability in OIR, implicating CA II as a therapeutic target for retinal edema.

In OIR, the molecular mechanisms of neuronal dysfunction are unknown. We observed altered expression of proteins that might be related to this mechanism. EAAT-1, also known as

GLAST, the major glutamate transporter of Müller cells, was downregulated in OIR P12 and P17 retinas.⁴⁵ Glutamate is transported into Müller cells by glutamate transporters and is converted into the nontoxic amino acid glutamine by glutamine synthetase.⁴⁵ Elevated extracellular glutamate is toxic to retinal neurons, suggesting that decreased EAAT-1 levels mediate glutamate toxicity in OIR. In addition, EAAT-1 is required in retinal signal transmission between photoreceptors and bipolar cells and has neuroprotective function during ischemia.⁴⁹ Thus, the downregulation of EAAT-1 is a possible mechanism of neuronal dysfunction in OIR.

Acyl-CoA-binding protein (ACBP), also known as diazepam-binding inhibitor, was upregulated in OIR P12 and P17 retinas. In the retina, ACBP is expressed and secreted by Müller cells and might regulate GABAergic activity, which is important for proper function of direction-selective retinal circuitry.^{50,51} The effect of increased ACBP levels on GABAergic transmission might be related to neuronal dysfunction in OIR.

Microtubule-associated protein 1 B (MAP1B) was downregulated in OIR P12 retinas but upregulated in OIR P17 retinas. MAP1B, a cytoskeletal element that is highly expressed in the developing nervous system, is believed to modulate the synaptic response in retinal neurons by interacting with specific subunits of retinal GABA_A receptors.⁵² Because MAP1B deficiency impairs neuronal activity, as demonstrated by decreased amplitude on electroretinograms, changes in MAP1B in OIR might also be related to neuronal dysfunction in OIR.⁵³

Further, LEDGF, a survival factor of the hepatoma-derived growth factor protein family, was also downregulated in OIR P17 retinas compared with OIR P12 retinas. LEDGF, a secreted protein that is induced by stress signals, localizes to the nucleus and activates stress-related genes.⁵⁴ Increased endogenous LEDGF and exogenous administration of LEDGF enhance the survival of retinal neurons.^{54,55} Thus, the downregulation of LEDGF might also accelerate neuronal dysfunction in OIR. The precise functions of EAAT-1, ACBP, MAP1B, and LEDGF in OIR are unknown, requiring further study.

Angiogenesis-related proteins, such as ORP150 and phosphoglycerate kinase (PGK1), were also upregulated in OIR in our study. ORP150, also known as hypoxia-upregulated protein 1 or glucose-regulated protein 170, is a 999-amino-acid protein that localizes to the endoplasmic reticulum (ER) and is a member of the heat shock protein 70 family.⁵⁶ In glioma cell lines, the inhibition of ORP150 expression decreases the release of VEGF, and in ORP150 antisense transfectants, VEGF accumulates in the ER, suggesting a critical function of the inducible ER chaperone ORP150 in tumor-mediated angiogenesis.⁵⁷ In our study, the retinal expression of ORP150 increased in OIR and colocalized to the neovascular tufts, implicating ORP150 in pathological retinal angiogenesis. Further, the knockdown of ORP150 by siRNA decreased the level of secreted VEGF in RPE cells, a major source of VEGF in the retina. Moreover, intravitreal administration of siRNA against ORP150 significantly reduced retinal neovascularization in OIR. Thus, the suppression of ORP150 appears to be a therapeutic goal for ameliorating neovascularization in ischemic retinopathy.

In retina, VEGF can be expressed by several cell types, including Müller cells, RPEs, vascular endothelial cells, ganglion cells, glial cells like astrocytes, and photoreceptors.⁵⁸ In OIR, VEGF is highly expressed in the neovascular tufts and the retinal GCL.⁵⁹ Also, VEGF receptor-2, one of the two VEGF receptor tyrosine kinases constitutively expressed in the inner nuclear layer and blood vessels in the GCL, is highly expressed in reforming retinal vessels and neovascular tufts in OIR.^{58,60} In retinal and choroidal pathological neovascularization, Müller cell- and RPE-derived VEGF are known to be crucial, respectively.^{61,62} In our study, ORP150 was expressed in the GCL, INL, RPE layer, and in the neovascular tufts. Müller cells span the entire thickness of the neural retina and the cell bodies lie in the INL. Reduced neovascularization by knock-down of ORP150 by siRNA in OIR might be explained by reduced VEGF secretion mainly from Müller glial cells. Also, VEGF from other glial cells, such as astrocytes, and ganglion cells might also be suppressed by knock-down of ORP150.

In addition, ORP150 has cytoprotective effects against ischemia/reperfusion injuries and neuroprotective effects against glutamate toxicity, which might be involved in the neurodegenerative mechanism in OIR, as shown in our study.^{63,64} In OIR, ORP150, which is expressed in the retinal GCL and INL, might also effect the stress response for neuronal survival. However, degeneration of retinal ganglion cell was not influenced by knock-down of ORP150.

PGK1, an ATP-generating glycolytic enzyme, is regulated by hypoxia-inducible factor-1 α , which also controls VEGF.⁶⁵ In prostate cancer cells, the overexpression of PGK1 lowers the secretion of VEGF and increases the generation of Angiostatin, which inhibits angiogenesis.⁶⁶ The upregulation and expression

in neovascular tufts of PGK1 in OIR might regulate retinal angiogenesis. However, its function in OIR is unknown.

In addition to the proteomic changes in OIR, our study generated comprehensive proteome profiles of developing mouse retinas from P12 and P17. The retinal vasculature remains immature until the end of the third postnatal week, and the neuronal system continues to develop during the first several weeks of life.^{67,68} Thus, proteome profiles with quantitation data contribute to research on retinal development.

Previous proteomic studies of retinal pathology revealed many differentially regulated proteins in animal models of diabetic retinopathy, optic nerve injury, and glaucoma.^{17,18,69–73} Many proteins such as Crystallin family were commonly identified in these studies. Similar to the results of our study, Crystallin α A, α B, β , and γ were upregulated in diabetic retina.¹⁸ On the contrary, in the optic nerve injury model, retinal Crystallin α A, β S, and β B2 were downregulated.⁷⁰ ACBP, which was upregulated in OIR, was also upregulated in diabetic retina and experimental glaucoma/ocular hypertension.^{69,72} EAAT-1, which was downregulated in OIR, was upregulated in diabetic retina and the optic nerve injury model.^{69,70} MAP1B, which was downregulated in OIR P12 retinas but upregulated in OIR P17 retinas, showed downregulation in the optic nerve injury model and no significant change in diabetic retina.^{69,71} The expression patterns of proteins in various retinal disease models may be helpful in understanding the functions of the proteins.

Because the retina is a multilayered, complex tissue that comprises at least 60 cell types, determining the immunohistochemical localization of differentially regulated proteins is essential for investigating their functions.⁷³ In our study, the upregulation of Crystallin proteins, vimentin, PGK1, and ORP150 has been demonstrated in immunohistochemical staining, but the downregulation of EAAT-1 and LEDGF by iTRAQ was not observed by immunohistochemistry. EAAT-1 and LEDGF are abundant proteins in Müller cells and retinal nuclear layers, respectively. Thus, despite the decreased expression of these proteins, they stained robustly, which precluded any comparison of the intensities.

Additional studies to determine the function of our proteins of interest are warranted. An examination of the effects of CA II inhibition on retinal vascular permeability, up- or downregulation of PGK1 on the secretion of VEGF and Angiostatin in retinal cells, administration of LEDGF in OIR models, and posttranslational modification of Crystallin proteins might facilitate identification of new potential therapeutic targets.

In conclusion, using a proteomics discovery method, coupled to targeted approaches, we identified many proteins that were differentially regulated in the mouse model of OIR, some of which might be involved in angiogenesis, vascular change, and neurodegeneration. Examining the differential regulation of the retinal proteome might increase our understanding of the pathophysiology of OIR. Specifically, ORP150 might be a new therapeutic target against retinal angiogenesis in ischemic proliferative retinopathy.

ASSOCIATED CONTENT

S Supporting Information

Supporting Tables S1–S4 showing the primary antibodies used for immunohistochemistry, identification of proteins from the iTRAQ experiments, differentially expressed proteins from the

iTRAQ experiments and identification of proteins from the LTQ Velos experiment. Supporting Figures S1–S10 showing Venn diagrams of identified proteins, classification of identified retinal proteins into “molecular function” subcategories, functional classification of differentially expressed proteins, identification of proteins from LTQ Velos experiments, immunolocalization of crystallin α A, crystallin β S, and LEDGF, immunolocalization of CA II and vimentin in OIR, immunolocalization of PGK1 in OIR, immunolocalization of ORP150 and Iba-1 OIR, immunolocalization of glutamine synthetase and vimentin after intravitreal injection of siRNA targeting ORP150, and density of retinal ganglion cells in OIR after intravitreal injection of siRNA targeting ORP150. This material is available free of charge via the Internet at <http://pubs.acs.org>.

■ AUTHOR INFORMATION

Corresponding Author

*(H.G.Y.) Tel: (+82) 2-2072-2438. Fax: (+82) 2-741-3187. E-mail: hgonyu@snu.ac.kr. (Y.K.) Tel: (+82) 2-740-8073. Fax: (+82) 2-741-0253. E-mail: biolab@snu.ac.kr.

Author Contributions

[#]These authors contributed equally to this work.

Notes

The authors declare no competing financial interest.

■ ACKNOWLEDGMENTS

This work was supported by a grant from the Seoul National University Hospital Research Fund (03-2010-0180), Midcareer Researcher Program (No. 2011-0027478), and the Converging Research Center Program (No. 2009-0094081, 2009-0093607) through the National Research Foundation of Korea (NRF), funded by the Ministry of Education, Science, and Technology.

■ REFERENCES

- (1) Sapieha, P.; Joyal, J. S.; Rivera, J. C.; Kermorvant-Duchemin, E.; Sennlaub, F.; Hardy, P.; Lachapelle, P.; Chemtob, S. Retinopathy of prematurity: understanding ischemic retinal vasculopathies at an extreme of life. *J. Clin. Invest.* **2010**, *120*, 3022–3032.
- (2) Cheung, N.; Mitchell, P.; Wong, T. Y. Diabetic retinopathy. *Lancet* **2010**, *376*, 124–136.
- (3) Wong, T. Y.; Scott, I. U. Clinical practice. Retinal-vein occlusion. *N. Engl. J. Med.* **2010**, *363*, 2135–2144.
- (4) Smith, L. E.; Shen, W.; Perruzzi, C.; Soker, S.; Kinose, F.; Xu, X.; Robinson, G.; Driver, S.; Bischoff, J.; Zhang, B.; Schaeffer, J. M.; Senger, D. R. Regulation of vascular endothelial growth factor-dependent retinal neovascularization by insulin-like growth factor-1 receptor. *Nat. Med.* **1999**, *5*, 1390–1395.
- (5) Smith, L. E.; Kopchick, J. J.; Chen, W.; Knapp, J.; Kinose, F.; Daley, D.; Foley, E.; Smith, R. G.; Schaeffer, J. M. Essential role of growth hormone in ischemia-induced retinal neovascularization. *Science* **1997**, *276*, 1706–1709.
- (6) Chen, J.; Connor, K. M.; Aderman, C. M.; Smith, L. E. Erythropoietin deficiency decreases vascular stability in mice. *J. Clin. Invest.* **2008**, *118*, 526–533.
- (7) Drixler, T. A.; BorelRinkes, I. H.; Ritchie, E. D.; Treffers, F. W.; van Vroonhoven, T. J.; Gebbink, M. F.; Voest, E. E. Angiostatin inhibits pathological but not physiological retinal angiogenesis. *Invest. Ophthalmol. Visual Sci.* **2001**, *42*, 3325–3330.
- (8) Stellmach, V.; Crawford, S. E.; Zhou, W.; Bouck, N. Prevention of ischemia-induced retinopathy by the natural ocular antiangiogenic agent pigment epithelium-derived factor. *Proc. Natl. Acad. Sci. U. S. A.* **2001**, *27*, 2593–2597.
- (9) Kojima, H.; Otani, A.; Oishi, A.; Makiyama, Y.; Nakagawa, S.; Yoshimura, N. Granulocyte colony-stimulating factor attenuates oxidative stress-induced apoptosis in vascular endothelial cells and exhibits functional and morphologic protective effect in oxygen-inducedretinopathy. *Blood* **2011**, *117*, 1091–1100.
- (10) Tang, Y.; Scheef, E. A.; Wang, S.; Sorenson, C. M.; Marcus, C. B.; Jefcoate, C. R.; Sheibani, N. CYP1B1 expression promotes the proangiogenic phenotype of endothelium through decreased intracellular oxidative stress and thrombospondin-2 expression. *Blood* **2009**, *113*, 744–754.
- (11) Kermorvant-Duchemin, E.; Sapieha, P.; Sirinyan, M.; Beauchamp, M.; Checchin, D.; Hardy, P.; Sennlaub, F.; Lachapelle, P.; Chemtob, S. Understanding ischemic retinopathies: emerging concepts from oxygen-inducedretinopathy. *Doc. Ophthalmol.* **2010**, *120*, 51–60.
- (12) Vessey, K. A.; Wilkinson-Berka, J. L.; Fletcher, E. L. Characterization of retinal function and glial cell response in a mouse model of oxygen-inducedretinopathy. *J. Comp. Neurol.* **2011**, *S19*, 506–527.
- (13) Tannu, N. S.; Hemby, S. E. Methods for proteomics in neuroscience. *Prog. Brain Res.* **2006**, *158*, 41–82.
- (14) Kim, S. J.; Kim, S.; Park, J.; Lee, H. K.; Park, K. S.; Yu, H. G.; Kim, Y. Differential expression of vitreous proteins in proliferative diabetic retinopathy. *Curr. Eye Res.* **2006**, *31*, 231–240.
- (15) Kim, T.; Kim, S. J.; Kim, K.; Kang, U. B.; Lee, C.; Park, K. S.; Yu, H. G.; Kim, Y. Profiling of vitreous proteomes from proliferative diabetic retinopathy and nondiabetic patients. *Proteomics* **2007**, *7*, 4203–4215.
- (16) Kim, K.; Kim, S. J.; Yu, H. G.; Yu, J.; Park, K. S.; Jang, I. J.; Kim, Y. Verification of biomarkers for diabetic retinopathy by multiple reaction monitoring. *J. Proteome Res.* **2010**, *9*, 689–699.
- (17) Gao, B. B.; Phipps, J. A.; Bursell, D.; Clermont, A. C.; Feener, E. P. Angiotensin AT1 receptor antagonism ameliorates murine retinal proteome changes induced by diabetes. *J. Proteome Res.* **2009**, *8*, 5541–5549.
- (18) Fort, P. E.; Freeman, W. M.; Losiewicz, M. K.; Singh, R. S.; Gardner, T. W. The retinal proteome in experimental diabetic retinopathy: up-regulation of crystallins and reversal by systemic and periocular insulin. *Mol. Cell. Proteomics* **2009**, *8*, 767–779.
- (19) Gao, B. B.; Chen, X.; Timothy, N.; Aiello, L. P.; Feener, E. P. Characterization of the vitreous proteome in diabetes without diabetic retinopathy and diabetes with proliferative diabetic retinopathy. *J. Proteome Res.* **2008**, *7*, 2516–2525.
- (20) Gao, B. B.; Clermont, A.; Rook, S.; Fonda, S. J.; Srinivasan, V. J.; Wojtkowski, M.; Fujimoto, J. G.; Avery, R. L.; Arrigg, P. G.; Bursell, S. E.; Aiello, L. P.; Feener, E. P. Extracellular carbonic anhydrase mediates hemorrhagic retinal and cerebral vascular permeability through prekallikrein activation. *Nat. Med.* **2007**, *13*, 181–188.
- (21) Smith, L. E.; Wesolowski, E.; McLellan, A.; Kostyk, S. K.; D'Amato, R.; Sullivan, R.; D'Amore, P. A. Oxygen-inducedretinopathy in the mouse. *Invest. Ophthalmol. Visual Sci.* **1994**, *35*, 101–111.
- (22) Penn, J. S.; Tolman, B. L.; Lowery, L. A. Variable oxygen exposure causes preretinal neovascularization in the newborn rat. *Invest. Ophthalmol. Visual Sci.* **1993**, *34*, 576–585.
- (23) Connor, K. M.; Krah, N. M.; Dennison, R. J.; Aderman, C. M.; Chen, J.; Guerin, K. I.; Sapieha, P.; Stahl, A.; Willett, K. L.; Smith, L. E. Quantification of oxygen-induced retinopathy in the mouse: a model of vessel loss, vessel regrowth and pathological angiogenesis. *Nat. Protoc.* **2009**, *4*, 1565–1573.
- (24) Grossniklaus, H. E.; Kang, S. J.; Berglin, L. Animal models of choroidal and retinal neovascularization. *Prog. Retinal Eye Res.* **2010**, *29*, 500–519.
- (25) Jin, J.; Kwon, Y. W.; Paek, J. S.; Cho, H. J.; Yu, J.; Lee, J. Y.; Chu, I. S.; Park, I. H.; Park, Y. B.; Kim, H. S.; Kim, Y. Analysis of differential proteomes of induced pluripotent stem cells by protein-based reprogramming of fibroblasts. *J. Proteome Res.* **2011**, *10*, 977–989.
- (26) Jin, J.; Park, J.; Kim, K.; Kang, Y.; Park, S. G.; Kim, J. H.; Park, K. S.; Jun, H.; Kim, Y. Detection of differential proteomes of human

- beta-cells during islet-like differentiation using iTRAQ labeling. *J. Proteome Res.* **2009**, *8*, 1393–1403.
- (27) Shilov, I. V.; Seymour, S. L.; Patel, A. A.; Loboda, A.; Tang, W. H.; Keating, S. P.; Hunter, C. L.; Nuwaysir, L. M.; Schaeffer, D. A. The Paragon Algorithm, a next generation search engine that uses sequence temperature values and feature probabilities to identify peptides from tandem mass spectra. *Mol. Cell. Proteomics* **2007**, *6*, 1638–1655.
- (28) Chu, V. T.; Gottardo, R.; Raftery, A. E.; Bumgarner, R. E.; Yeung, K. Y. MeV+R: using MeV as a graphical user interface for Bioconductor applications in microarray analysis. *Genome Biol.* **2008**, *9*, R118.
- (29) Keller, A.; Nesvizhskii, A. I.; Kolker, E.; Aebersold, R. Empirical statistical model to estimate the accuracy of peptide identifications made by MS/MS and database search. *Anal. Chem.* **2002**, *74*, 5383–5392.
- (30) Nesvizhskii, A. I.; Keller, A.; Kolker, E.; Aebersold, R. A statistical model for identifying proteins by tandem mass spectrometry. *Anal. Chem.* **2003**, *75*, 4646–4658.
- (31) Lim, Y.; Jo, D. H.; Kim, J. H.; Ahn, J. H.; Hwang, Y. K.; Kang, D. K.; Chang, S. I.; Yu, Y. S.; Yoon, Y.; Kim, J. H. Human apolipoprotein(a) kringle V inhibits ischemia-induced retinal neovascularization via suppression of fibronectin-mediated angiogenesis. *Diabetes* **2012**, *61*, 1599–1608.
- (32) Goto, W.; Ota, T.; Morikawa, N.; Otori, Y.; Hara, H.; Kawazu, K.; Miyawaki, N.; Tano, Y. Protective effects of timolol against the neuronal damage induced by glutamate and ischemia in the rat retina. *Brain Res.* **2002**, *958*, 10–19.
- (33) Seki, M.; Tanaka, T.; Matsuda, H.; Togano, T.; Hashimoto, K.; Ueda, J.; Fukuchi, T.; Abe, H. Topically administered timolol and dorzolamide reduce intraocular pressure and protect retinal ganglion cells in a rat experimental glaucoma model. *Br. J. Ophthalmol.* **2005**, *89*, 504–507.
- (34) Han, C. L.; Chen, J. S.; Chan, E. C.; Wu, C. P.; Yu, K. H.; Chen, K. T.; Tsou, C. C.; Tsai, C. F.; Chien, C. W.; Kuo, Y. B.; Lin, P. Y.; Yu, J. S.; Hsueh, C.; Chen, M. C.; Chan, C. C.; Chang, Y. S.; Chen, Y. J. An informatics-assisted label-free approach for personalized tissue membrane proteomics: case study on colorectal cancer. *Mol. Cell. Proteomics* **2011**, DOI: 10.M110.003087.
- (35) Ecroyd, H.; Meehan, S.; Horwitz, J.; Aquilina, J. A.; Benesch, J. L.; Robinson, C. V.; Macphee, C. E.; Carver, J. A. Mimicking phosphorylation of alphaB-Crystallin affects its chaperone activity. *Biochem. J.* **2007**, *401*, 129–141.
- (36) Weiwei, Z.; Hu, R. Targeting carbonic anhydrase to treat diabetic retinopathy: emerging evidences and encouraging results. *Biochem. Biophys. Commun.* **2009**, *390*, 368–371.
- (37) Kase, S.; He, S.; Sonoda, S.; Kitamura, M.; Spee, C.; Wawrousek, E.; Ryan, S. J.; Kannan, R.; Hinton, D. R. alphaB-Crystallin regulation of angiogenesis by modulation of VEGF. *Blood* **2010**, *115*, 3398–3406.
- (38) Fort, P. E.; Lampi, K. J. New focus on alpha-crystallins in retinal neurodegenerative diseases. *Exp. Eye Res.* **2011**, *92*, 98–103.
- (39) Sakaguchi, H.; Miyagi, M.; Darrow, R. M.; Crabb, J. S.; Hollyfield, J. G.; Organisciak, D. T.; Crabb, J. W. Intense light exposure changes the Crystallin content in retina. *Exp. Eye Res.* **2003**, *76*, 131–133.
- (40) Vázquez-Chona, F.; Song, B. K.; Geisert, E. E., Jr. Temporal changes in gene expression after injury in the rat retina. *Invest. Ophthalmol. Visual Sci.* **2004**, *45*, 2737–2746.
- (41) Munemasa, Y.; Kwong, J. M.; Caprioli, J.; Piri, N. The role of alphaA- and alphaB-crystallins in the survival of retinal ganglion cells after optic nerve axotomy. *Invest. Ophthalmol. Visual Sci.* **2009**, *50*, 3869–3875.
- (42) Piri, N.; Song, M.; Kwong, J. M.; Caprioli, J. Modulation of alpha and beta Crystallin expression in rat retinas with ocular hypertension-induced ganglion cell degeneration. *Brain Res.* **2007**, *1141*, 1–9.
- (43) Liedtke, T.; Schwamborn, J. C.; Schröer, U.; Thanos, S. Elongation of axons during regeneration involves retinal Crystallin beta b2 (crybb2). *Mol. Cell. Proteomics* **2007**, *6*, 895–907.
- (44) Sinha, D.; Esumi, N.; Jaworski, C.; Kozak, C. A.; Pierce, E.; Wistow, G. Cloning and mapping the mouse Crygs gene and non-lens expression of [gamma]S-Crystallin. *Mol. Vision* **1998**, *4*, 8.
- (45) Bringmann, A.; Pannicke, T.; Grosche, J.; Francke, M.; Wiedemann, P.; Skatchkov, S. N.; Osborne, N. N.; Reichenbach, A. Müller cells in the healthy and diseased retina. *Prog. Retinal Eye Res.* **2006**, *25*, 397–424.
- (46) Bringmann, A.; Iandiev, I.; Pannicke, T.; Wurm, A.; Hollborn, M.; Wiedemann, P.; Osborne, N. N.; Reichenbach, A. Cellular signaling and factors involved in Müller cell gliosis: neuroprotective and detrimental effects. *Prog. Retinal Eye Res.* **2009**, *28*, 423–451.
- (47) Nagelhus, E. A.; Mathiisen, T. M.; Bateman, A. C.; Haug, F. M.; Ottersen, O. P.; Grubb, J. H.; Waheed, A.; Sly, W. S. Carbonic anhydrase XIV is enriched in specific membrane domains of retinal pigment epithelium, Müller cells, and astrocytes. *Proc. Natl. Acad. Sci. U. S. A.* **2005**, *102*, 8030–8035.
- (48) Weiwei, Z.; Hu, R. Targeting carbonic anhydrase to treat diabetic retinopathy: emerging evidences and encouraging results. *Biochem. Biophys. Res. Commun.* **2009**, *390*, 368–371.
- (49) Harada, T.; Harada, C.; Watanabe, M.; Inoue, Y.; Sakagawa, T.; Nakayama, N.; Sasaki, S.; Okuyama, S.; Watase, K.; Wada, K.; Tanaka, K. Functions of the two glutamate transporters GLAST and GLT-1 in the retina. *Proc. Natl. Acad. Sci. U. S. A.* **1998**, *95*, 4663–4666.
- (50) Barmack, N. H.; Bilderback, T. R.; Liu, H.; Qian, Z.; Yakhnitsa, V. Activity-dependent expression of acyl-coenzyme a-bindingprotein in retinal muller glial cells evoked by optokinetic stimulation. *J. Neurosci.* **2004**, *24*, 1023–1033.
- (51) Qian, Z.; Bilderback, T. R.; Barmack, N. H. Acyl coenzyme A-binding protein (ACBP) is phosphorylated and secreted by retinal Müller astrocytes following protein kinase C activation. *J. Neurochem.* **2008**, *105*, 1287–1299.
- (52) Hanley, J. G.; Koulen, P.; Bedford, F.; Gordon-Weeks, P. R.; Moss, S. J. The protein MAP-1B links GABA(C) receptors to the cytoskeleton at retinal synapses. *Nature* **1999**, *397*, 66–69.
- (53) Pangratz-Fuehrer, S.; Bubna-Littitz, H.; Propst, F.; Reitsamer, H. Mice deficient in microtubule-associated proteinMAP1B show a distinct behavioral phenotype and altered retina function. *Behav. Brain Res.* **2005**, *164*, 188–196.
- (54) Shinohara, T.; Singh, D. P.; Fatma, N. LEDGF, a survival factor, activates stress-related genes. *Prog. Retinal Eye Res.* **2002**, *21*, 341–358.
- (55) Raz-Prag, D.; Zeng, Y.; Sieving, P. A.; Bush, R. A. Photoreceptor protection by adeno-associated virus-mediated LEDGF expression in the RCS rat model of retinal degeneration: probing the mechanism. *Invest. Ophthalmol. Visual Sci.* **2009**, *50*, 3897–3906.
- (56) Kuwabara, K.; Matsumoto, M.; Ikeda, J.; Hori, O.; Ogawa, S.; Maeda, Y.; Kitagawa, K.; Imuta, N.; Kinoshita, T.; Stern, D. M.; Yanagi, H.; Kamada, T. Purification and characterization of a novel stress protein, the 150-kDa oxygen-regulated protein (ORP150), from cultured rat astrocytes and its expression in ischemic mouse brain. *J. Biol. Chem.* **1996**, *271*, 5025–5032.
- (57) Ozawa, K.; Tsukamoto, Y.; Hori, O.; Kitao, Y.; Yanagi, H.; Stern, D. M.; Ogawa, S. Regulation of tumor angiogenesis by oxygen-regulated protein 150, an inducible endoplasmic reticulum chaperone. *Cancer Res.* **2001**, *61*, 4206–4213.
- (58) Kim, I.; Ryan, A. M.; Rohan, R.; Amano, S.; Aguilar, S.; Miller, J. W.; Adamis, A. P. Constitutive expression of VEGF, VEGFR-1, and VEGFR-2 in normal eyes. *Invest. Ophthalmol. Visual Sci.* **1999**, *40*, 2115–2121.
- (59) Zhao, M.; Shi, X.; Liang, J.; Miao, Y.; Xie, W.; Zhang, Y.; Li, X. Expression of pro- and anti-angiogenic isoforms of VEGF in the mouse model of oxygen-induced retinopathy. *Exp. Eye Res.* **2011**, *93*, 921–926.
- (60) McLeod, D. S.; Taomoto, M.; Cao, J.; Zhu, Z.; Witte, L.; Lutty, G. A. Localization of VEGF receptor-2 (KDR/Flk-1) and effects of blocking it in oxygen-induced retinopathy. *Invest. Ophthalmol. Visual Sci.* **2002**, *43*, 474–482.
- (61) Bai, Y.; Ma, J. X.; Guo, J.; Wang, J.; Zhu, M.; Chen, Y.; Le, Y. Z. Müller cell-derived VEGF is a significant contributor to retinal neovascularization. *J. Pathol.* **2009**, *219*, 446–454.

- (62) Spilsbury, K.; Garrett, K. L.; Shen, W. Y.; Constable, I. J.; Rakoczy, P. E. Overexpression of vascular endothelial growth factor (VEGF) in the retinal pigment epithelium leads to the development of choroidal neovascularization. *Am. J. Pathol.* **2000**, *157*, 135–144.
- (63) Kitao, Y.; Ozawa, K.; Miyazaki, M.; Tamatani, M.; Kobayashi, T.; Yanagi, H.; Okabe, M.; Ikawa, M.; Yamashima, T.; Stern, D. M.; Hori, O.; Ogawa, S. Expression of the endoplasmic reticulum molecular chaperone (ORP150) rescues hippocampal neurons from glutamate toxicity. *J. Clin. Invest.* **2001**, *108*, 1439–1450.
- (64) Kitano, H.; Nishimura, H.; Tachibana, H.; Yoshikawa, H.; Matsuyama, T. ORP150 ameliorates ischemia/reperfusion injury from middle cerebral artery occlusion in mouse brain. *Brain Res.* **2004**, *1015*, 122–128.
- (65) Semenza, G. L.; Roth, P. H.; Fang, H. M.; Wang, G. L. Transcriptional regulation of genes encoding glycolytic enzymes by hypoxia-inducible factor 1. *J. Biol. Chem.* **1994**, *269*, 23757–23763.
- (66) Wang, J.; Wang, J.; Dai, J.; Jung, Y.; Wei, C. L.; Wang, Y.; Havens, A. M.; Hogg, P. J.; Keller, E. T.; Pienta, K. J.; Nor, J. E.; Wang, C. Y.; Taichman, R. S. A glycolytic mechanism regulating an angiogenic switch in prostate cancer. *Cancer Res.* **2007**, *67*, 149–159.
- (67) Stahl, A.; Connor, K. M.; Sapieha, P.; Chen, J.; Dennison, R. J.; Krah, N. M.; Seaward, M. R.; Willett, K. L.; Aderman, C. M.; Guerin, K. I.; Hua, J.; Löfqvist, C.; Hellström, A.; Smith, L. E. The mouseretina as an angiogenesis model. *Invest. Ophthalmol. Visual Sci.* **2010**, *51*, 2813–2826.
- (68) Coombs, J. L.; Van Der List, D.; Chalupa, L. M. Morphological properties of mouse retinal ganglion cells during postnatal development. *J. Comp. Neurol.* **2007**, *503*, 803–814.
- (69) VanGuilder, H. D.; Bixler, G. V.; Kutzler, L.; Brucklacher, R. M.; Bronson, S. K.; Kimball, S. R.; Freeman, W. M. Multi-modal proteomic analysis of retinal protein expression alterations in a rat model of diabetic retinopathy. *PLoS One* **2011**, *6*, e16271.
- (70) Magharious, M.; D'Onofrio, P. M.; Hollander, A.; Zhu, P.; Chen, J.; Koeberle, P. D. Quantitative iTRAQ analysis of retinal ganglion cell degeneration after optic nerve crush. *J. Proteome Res.* **2011**, *10*, 3344–3362.
- (71) Hollander, A.; D'Onofrio, P. M.; Magharious, M. M.; Lysko, M. D.; Koeberle, P. D. Quantitative retinal protein analysis after optic nerve transection reveals a neuroprotective role for hepatoma-derived growth factor on injured retinal ganglion cells. *Invest. Ophthalmol. Visual Sci.* **2012**, *53*, 3973–3989.
- (72) Crabb, J. W.; Yuan, X.; Dvoriantchikova, G.; Ivanov, D.; Crabb, J. S.; Shestopalov, V. I. Preliminary quantitative proteomic characterization of glaucomatous rat retinal ganglion cells. *Exp. Eye Res.* **2010**, *91*, 107–110.
- (73) Kolb, H.; Nelson, R.; Ahnelt, P.; Cuenca, N. Cellular organization of the vertebrate retina. *Prog. Brain Res.* **2001**, *131*, 3–26.